



BRNO UNIVERSITY OF TECHNOLOGY

FACULTY OF CIVIL ENGINEERING

FATIGUE PROPERTIES OF STEEL S355

BACHELOR THESIS

AUTHOR

D. Álvaro Martín González

SUPERVISOR

Assoc. Prof. Stanislav Seitl, Ph. D.

SUPERVISOR SPECIALIST:

Ing. Petr Miarka

BRNO, CZECH REPUBLIC 2018

ABSTRACT

This thesis is focused in the numerical simulation by software ANSYS (finite elements method) of fatigue properties such as the Wöhler's curves and crack propagation rates and Fracture Mechanics properties such as stress intensity factors and T -stresses in Compact Tension specimen.

Two grades of structural steel S355 will be evaluated in order to study the influence of the material in the fatigue properties.

Calibration curves will be used for evaluation of data, comparing the results with data published in literature.

KEYWORDS

Fatigue, Finite Element Method, Fracture Mechanics, Stress Intensity Factor, T -stress, Crack Propagation Rate, Wöhler's Curves, Compact Tension Specimen, Structural Steel S355, ASTM, EN.

RESUMEN

Este proyecto se basa en la simulación numérica con ANSYS (software para el análisis mediante el método de los elementos finitos) de propiedades de la fatiga tales como las curvas de Wöhler y velocidades de propagación de grieta, y propiedades de la Mecánica de la Fractura tales como factores intensidad de tensiones y tensiones- T mediante probetas CT (del inglés, *Compact Tension*).

Se evaluarán dos grados diferentes de acero estructural S355 con la finalidad de estudiar la influencia del material en dichas propiedades.

Para la evaluación de los resultados numéricos se utilizarán curvas de calibración, comparando, los mismos, con datos publicados en diferentes artículos.

PALABRAS CLAVE

Fatiga, Método de los Elementos Finitos, Mecánica de la Fractura, Factor Intensidad de Tensiones, Tensión T , Velocidad de Propagación de Grieta, Curvas de Wöhler, Probeta CT, Acero Estructural S355, ASTM, EN.

BIBLIOGRAPHIC CITATION

Álvaro Martín González, *Fatigue properties of steel S355 measured by Compact Tension test*. Brno, 2018. 63 p., 9 p. of attachments. Bachelor Thesis. Brno University of Technology, Faculty of civil engineering, Supervisor: Assoc. Prof. Stanislav Seitzl, Ph. D. Supervisor Specialist: Ing. Petr Miarka.

The present thesis is the final part of my studies in Mechanical Engineering (2014-2018) at the University of Oviedo. It has been held in Brno, Czech Republic, during Erasmus+ mobility in collaboration with staff from Faculty of civil engineering, Brno University of Technology.

I would like to thank the invaluable help of my tutors, who have made it possible for me to carry out this project; Stanislav Seitzl, Petr Miarka and María Jesús Lamela Rey. Also, to my parents and my sister. It would not have been possible to carry out this project without their help and support.

ACKNOWLEDGEMENT

The author acknowledges the support of Czech Sciences Foundation project under the contract **No. 17-01589S**. This thesis has been carried out under the project **No. LO1408** "AdMaS UP – Advanced Materials, Structures and Technologies", supported by Ministry of Education, Youth and Sports under the „National Sustainability Programme I”.

INDEX

1. INTRODUCTION	7
2. THEORETICAL BACKGROUND	8
2.1 Linear Elastic Fracture Mechanics.....	8
2.1.1 <i>The stress analysis of cracks</i>	8
2.1.2 <i>The stress intensity factor</i>	9
2.1.3 <i>T-stress</i>	10
2.1.4 <i>Crack-tip plasticity</i>	10
2.2 Elastic-Plastic Fracture Mechanics.....	11
2.2.1 <i>Crack-Tip Opening Displacement</i>	11
2.3 Fatigue.....	12
2.3.1 <i>Fatigue regimes</i>	12
2.3.2 <i>Fatigue failure models</i>	12
2.3.3 <i>The Compact Test specimen (ASTM E647)</i>	24
2.3.4 <i>Structural steel S355 (EN 10025)</i>	26
3. AIM OF THESIS	30
4. NUMERICAL MODELING IN ANSYS.....	31
4.1 Prior set up.....	31
4.2 Pre-processor.....	31
4.2.1 <i>Specimen</i>	31
4.2.2 <i>Element type</i>	31
4.2.3 <i>Material</i>	32
4.2.4 <i>Modelling of the specimen</i>	33
4.2.5 <i>Meshing</i>	37
4.2.6 <i>Boundary conditions</i>	37
4.3 Solve.....	38
4.4 Post-processor.....	40
4.4.1 <i>Stress Intensity Factor</i>	40
4.4.2 <i>T-stress</i>	41
5. NUMERICAL RESULTS	43
5.1 Stress Intensity Factors.....	43

5.1.1	ASTM literature calculations.....	43
5.1.2	Knésl and Bednar literature calculations.....	44
5.1.3	ANSYS calculations.....	44
5.2	<i>T</i> -stresses.....	45
5.2.1	Knésl and Bednar literature calculations.....	45
5.2.2	ANSYS calculations.....	46
6.	VALUES OF S355 PUBLISHED IN LITERATURE.....	48
6.1	Experimental data of <i>S-N</i> curves published in literature.....	48
6.2	Experimental data of crack propagation rates published in literature.....	49
7.	EVALUATION OF S355 MEASURED DATA AT INSTITUTE OF PHYSICS OF MATERIALS.....	50
7.1	Experimental data of <i>S-N</i> curves from IPM.....	50
7.2	Experimental data of crack propagation rates from IPM.....	52
8.	COMPARISON AND DISCUSSION OF THE RESULTS.....	55
8.1	Comparison of curves from ANSYS and literature.....	55
8.1.1	Comparison of Stress Intensity Factor.....	55
8.1.2	Comparison of <i>T</i> -stress.....	56
8.2	Comparison of Stress-Number of cycles curves.....	56
8.3	Comparison of crack propagation rate curves.....	58
9.	CONCLUSIONS.....	59
10.	APPENDIX.....	60
10.1	APPENDIX I - Nomenclature.....	60
10.2	APPENDIX II - List of figures.....	61
10.3	APPENDIX III - List of tables.....	62
10.4	APPENDIX IV - List of graphs.....	63
10.5	APPENDIX V - Macro for the CT specimen.....	65
10.5.1	Prior setup.....	65
10.5.2	Preprocessor.....	65
10.5.3	Solve.....	67
10.5.4	Postprocessing.....	67
11.	REFERENCES.....	69
12.	CURRICULUM VITAE.....	71

1. INTRODUCTION

In general, perhaps fatigue is the most important failure mode to be considered in mechanical and structural design. For some products, fatigue accounts for more than 80 % of all observed service failures.

Moreover, fatigue and fracture failures are sometimes catastrophic, occurring without warning and causing significant property damage and loss of life. Design for fatigue avoidance is difficult because the fatigue stresses are complicated random processes, the fatigue process is influenced by many factors, and many of the factors are subjected to considerable uncertainty. [1]

Structural steel and, in particular, mild steel such as S355, is used for bolts, chains, connecting rods, and, in civil engineering, for railroad axes, and metallic structures (such as towers and bridges), i.e. allows designing lighter, slenderer and simpler structures with high structural performance.

When those large structures are designed and built, different individual components are used and joined together (usually by welding). In these situations, it does not matter what care you have and how stricter is the quality control applied, the existence of small defects (cracks) is unavoidable. The dimensions of the pre-existing cracks are usually defined by the detection limit of the non-destructive testing method applied in quality control after manufacturing or in regular inspections in service. [2]

Since the first research on metal fatigue began in the 18th century (Wilhelm Albert [3]), a very large number of researchers from all over the world have contributed to the knowledge base that has been amassed.

By far, the most influential person at the beginning of the systematic study of fatigue was August Wöhler.

The study of *fracture mechanics*, which describe the physics and mathematics behind the growth of cracks in brittle solids, was begun by Alan Griffith in 1921 [4] but is in the early 1960s when Paris and others [5] demonstrated that fracture mechanics is a useful tool for characterizing crack growth by fatigue. Since that time, the application of fracture mechanics to fatigue problems has become routine.

On the other hand, the major advance in the *statistical treatment* of fatigue data occurred with the work of Waloddi Weibull in the late 1930's [6]. Also, the ASTM has played an active role in development of statistical methods of fatigue data analysis dating back to 1951 [7], [8].

Because of this, fatigue problems have been traditionally faced from two different points of view: the Wöhler's curves-based (statistical) and the fracture mechanics-based approaches, that constitute two complementary but comprehensive methods to face fatigue lifetime prediction of mechanical and structural elements.

2. THEORETICAL BACKGROUND

2.1 Linear Elastic Fracture Mechanics

Linear elastic fracture mechanics (LEFM) is valid only as long as nonlinear material deformation is confined to a small region surrounding the crack tip.

There are two approaches to linear elastic fracture mechanics: the energy (G) and stress intensity. In the case of the perfectly elastic materials, both factors are related in Equation (1). This thesis is not focused in the energy approach.

$$G = \frac{K^2}{E'} \quad (1)$$

where:

$E' = E$ Young's modulus for plane stress and

$E' = \frac{E}{1-\vartheta}$ Young's modulus for plane strain, where ϑ is Poisson's ratio.

Griffith observed in 1920 that the discrepancy between the actual strengths of brittle materials and theoretical estimates was due to flaws in these materials. Fracture cannot occur unless the stress at the atomic level exceeds the cohesive strength of the material. Thus, the flaws must lower the global strength by magnifying the stress locally.

2.1.1 The stress analysis of cracks

If we define a Polar coordinate axis with the origin at the crack tip (Figure 1), it can be shown that the stress field in any linear elastic cracked body is given by:

$$\sigma_{ij} = \left(\frac{k}{\sqrt{r}}\right) f_{ij}(\theta) + \sum_{m=0}^{\infty} A_m r^{\frac{m}{2}} g_{ij}^{(m)}(\theta), \quad (2)$$

where:

σ_{ij} = stress tensor,

r and θ are Polar coordination as defined in Figure 1,

k = constant and

f_{ij} = dimensionless function of θ in the leading term.

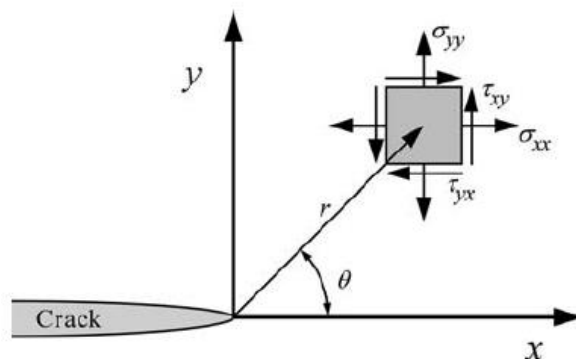


Figure 1-Definition of the coordinate system with origin in crack tip: Polar and Cartesian. [9]

Therefore, a stress singularity exists at the tip of an elastic crack because the stress field in any linear elastic cracked body solution contains a leading term that is proportional to $\frac{1}{\sqrt{r}}$. As $r \rightarrow 0$, the leading term approaches infinity so stress is asymptotic to $r = 0$ (regardless of the configuration of the cracked body) as shown in Equation (2).

2.1.2 The stress intensity factor

There are three types of loading that a crack can experience, as Figure 2 illustrates. *Mode I* loading, where the principal load is applied normal to the crack plane, tends to open the crack. *Mode II* corresponds to in-plane shear loading and tends to slide one crack face with respect to the other. *Mode III* refers to out-of-plane shear. A cracked body can be loaded in any one of these modes, or a combination of two or three modes.

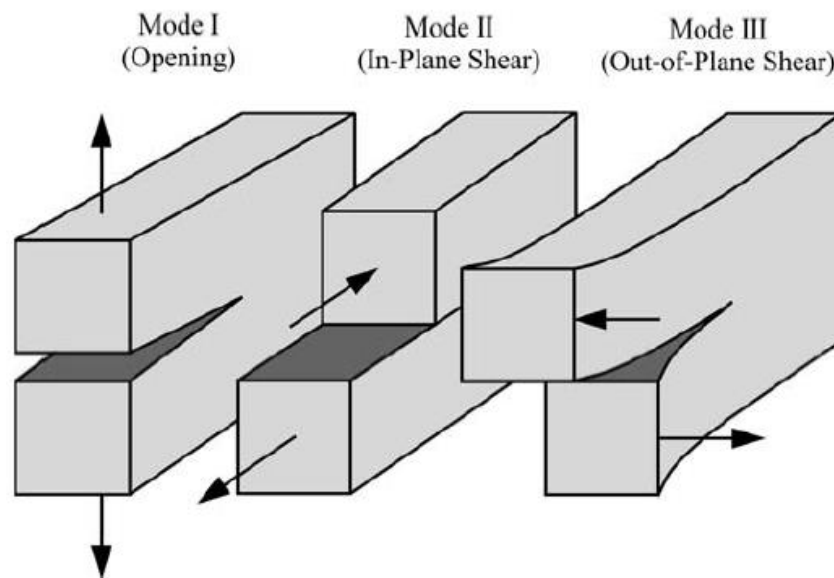


Figure 2-The three modes of loading that a crack can experience. [9]

Each mode of loading produces the singularity at the crack tip, but the proportionality constants k and f_{ij} depend on the mode. It is convenient at this point to replace k by the *stress intensity factor (SIF) K*, where $K = k\sqrt{2\pi}$. The stress intensity factor is usually given a subscript to denote the mode of loading, i.e., K_I , K_{II} , or K_{III} .

The stress intensity factor defines the amplitude of the crack-tip singularity. That is, stresses near the crack tip increase in proportion to K . Moreover, the stress intensity factor completely defines the crack tip conditions; if K is known, it is possible to solve for all components of stress, strain, and displacement as a function of r and θ . This single-parameter description of crack tip conditions turns out to be one of the most important concepts in fracture mechanics.

In this thesis, only pure *Mode I* is considered, since in the evaluation with Compact Tension Specimen, the load is applied normal to the crack plane. Because of this, in the following, when referring to "SIF", it is understood K_I .

2.1.3 *T*-stress

T-stress is used as a second parameter to fully characterize the crack tip. Generally, the SIF is enough, but there are some cases where conventional LEFM fails and, then, *T*-stress plays its role.

This parameter, in plane conditions, represents the stress acting parallel to the crack tip in the *x*-direction.

The *T*-stress factor can have a significant effect on the size and shape of the plastic zone that develops around the crack.

T-stress may be determined from analytical solutions after series expansion of the stress field. In the case of numerical modelling, the *T*-stress is usually determined as the medium value of the tensile or compressive stresses acting in the two flank sides of the crack. Using another method, the *T*-stress results, for $\theta = 0$ in Polar coordinates (Figure 3), from:

$$T = \lim_{r \rightarrow 0} (\sigma_{xx} - \sigma_{yy})_{\theta=0}, \quad (3)$$

where:

σ_{xx} stress as defined in Figure 3 for $\theta=0^\circ$ and

σ_{yy} stress as defined in Figure 3 for $\theta=0^\circ$.

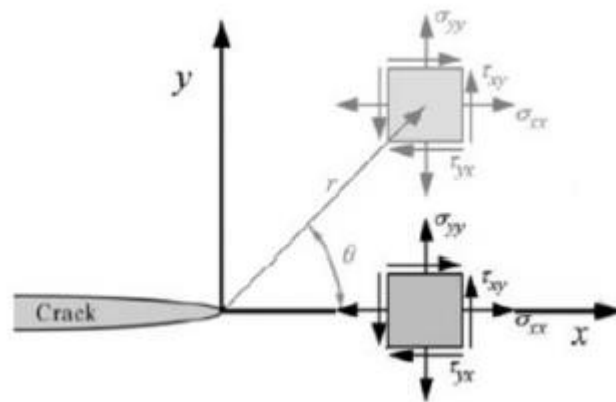


Figure 3-Definition of Polar coordinates with $\theta = 0$ [9]

2.1.4 Crack-tip plasticity

Linear elastic stress analysis of sharp cracks predicts infinite stresses at the crack tip. In practice, materials (especially metals) tend to exhibit a yield stress, above which they deform plastically. This means that there is always a region around the tip of a crack in a metal, where plastic deformation occurs, and hence a stress singularity cannot exist. The plastic region is known as the crack tip plastic zone.

The size of the crack-tip-yielding zone can be estimated by two methods: the Irwin approach, where the elastic stress analysis is used to estimate the elastic-plastic boundary, and the strip-yield model. Both approaches lead to simple corrections for crack-tip yielding. The term "plastic zone" usually applies to metals.

2.2 Elastic-Plastic Fracture Mechanics

Elastic-plastic fracture mechanics (EPFM) applies to materials that exhibit time-independent, nonlinear behavior (i.e., plastic deformation).

As in LEFM, there exists two approaches: the crack-tip-opening displacement (CTOD) and the J contour integral (energetic criterion).

2.2.1 Crack-Tip Opening Displacement

In the process of loading an elastoplastic material that has a sharp crack, due to the large plastic area developed in the front of the crack, it is flattened, as shown in Figure 4. The opening at the end of the crack, δ , is known as Crack Tip Opening Displacement (CTOD) and it has been shown that this value, at the time of breakage, is greater the more tough the material in question is.

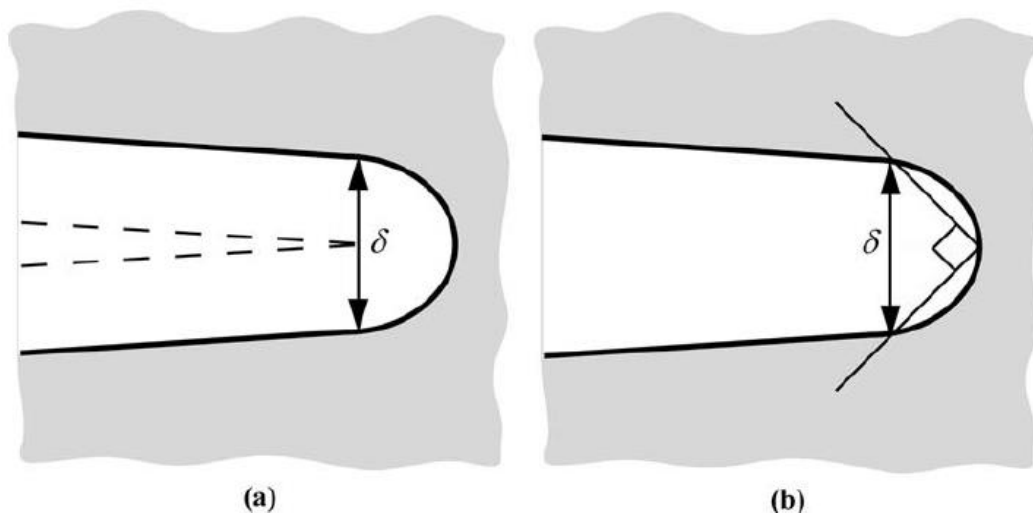


Figure 4-Alternative definitions of CTOD: (a) displacement at the original crack tip and (b) displacement at the intersection of a 90° vertex with the crack flanks. [9]

It is possible to compute the CTOD (δ) in the case of a solid with linear elastic behavior and it has been shown that in this case, a direct relationship between this parameter and the SIF occurs:

$$\delta = \frac{K^2}{\lambda \sigma_{ys} E'} \quad (4)$$

where:

λ is a constant that varies between 1 (plane stress) and 2 (plane strain) and E' as defined in Equation (1)

The EPFM, and then the CTOD and J parameters, are valid to characterize the crack tip behavior until an excessive plasticity or a big-scale deformation exists.

2.3 Fatigue

2.3.1 Fatigue regimes

There exist several regimes depending on the number of cycles (approximately) an element is subjected to (as can be shown in Graph 1):

Very Low-Cycle Fatigue (VLCF): $N_f < 10^2$ cycles

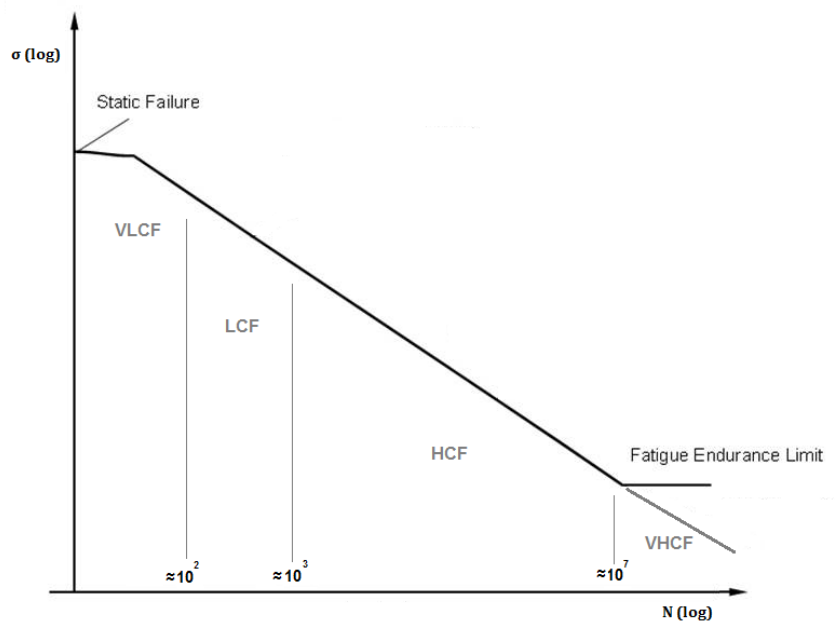
Low-Cycle Fatigue (LCF): $10^2 < N_f < 10^3$ cycles

High-Cycle Fatigue (HCF): $10^3 < N_f < 10^7$ cycles

Very High-Cycle Fatigue (VHCF): $N_f > 10^7$ cycles

This classification is convenient from the point of view of the application of fatigue failure models.

Usually, mechanical engineering structures are designed for high- (HCF) and low-cycle fatigue (LCF) regimes. Civil engineering structures such as bridges, are designed for high-cycle fatigue (HCF) regime.



Graph 1-Fatigue regimes.

2.3.2 Fatigue failure models

As said in the introduction, fatigue problems have been traditionally faced from two different points of view: the Wöhler's curves-based and the fracture mechanics-based approaches, that constitute two complementary but comprehensive methods to face fatigue lifetime prediction of mechanical and structural elements. Depending on the specific problem being solved, one of them is selected:

-The Wöhler's curves-based models.

-The fracture mechanics-based models.

Even though these two approaches have been normally considered separately and the connection between them has been obviated, so that many researchers consider

them as two completely different problems, in Castillo et al. [10] a clear connection between the two models is presented, showing that they share common information, which is useful in applications.

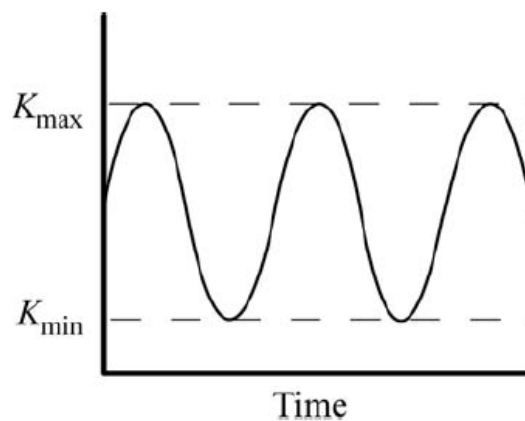
2.3.2.1 Fracture mechanics approach

The crack-growth curves are of interest for this approach. This approach is suitable for LCF regimes.

➤ The functional-relationships of the crack growth per cycle

- Fatigue crack growth under constant amplitude and small-scale yielding (f_1)

As can be shown in Figure 5, cyclic plastic zone forms at the crack tip, and the growing crack leaves behind a plastic wake. If the plastic zone is sufficiently small (small-scale yielding) that it is embedded within an elastic singularity zone, the conditions at the crack tip are uniquely defined by the current K value, and the crack growth rate is characterized by K_{max} and K_{min} (Graph 2). Constant amplitude means $(dK/d\alpha) = 0$.



Graph 2-Constant amplitude fatigue crack growth. [9]

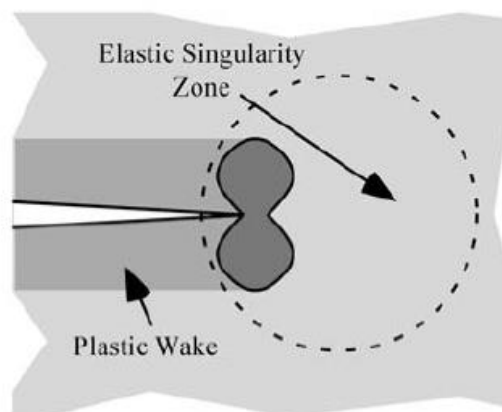


Figure 5-Small-scale yielding condition. [9]

The functional relationship for crack growth can be expressed as:

$$\frac{da}{dN} = f_1(\Delta K, R), \quad (5)$$

where:

$$\Delta K = (K_{max} - K_{min}),$$

$$R = \frac{K_{min}}{K_{max}} \text{ and}$$

$$\frac{da}{dN} = \text{crack growth per cycle,}$$

- Fatigue crack growth under variable amplitude (f_2)

If K_{max} or K_{min} varies during cyclic loading, the crack growth in a given cycle depend on the loading history as well as the current values of K_{min} and K_{max} .

The functional relationship for crack growth can be, then, expressed as:

$$\frac{da}{dN} = f_2(\Delta K, R, \mathcal{H}), \quad (6)$$

where:

\mathcal{H} = history dependence, which results from prior plastic deformation.

Similitude of crack-tip conditions, which implies a *unique* relationship among $\frac{da}{dN}$, ΔK , and R , is rigorously valid only for constant amplitude loading, as explained in the previous item (2.2.1).

Variable amplitude fatigue analyses that account for prior loading history are considerably more cumbersome than analyses that assume similitude. Therefore, the latter type of analysis is desirable if the similitude assumption is justified. There are many practical situations where such an assumption is reasonable. Such cases normally involve cyclic loading at high R ratios, where crack closure effects are negligible. Steel bridges, for example, have high dead loads due to their own weight, which translates into high R ratios. Also fatigue of welds that have not been stress relieved often obey similitude because tensile residual stresses, which are static, increase the effective R ratio.

- Fatigue crack growth under large-scale plasticity (f_3)

This is the second case where the similitude is violated since K no longer characterizes the crack-tip conditions in such cases. Is the J contour integral.

The functional relationship for crack growth can be, then, expressed as:

$$\frac{da}{dN} = f_3(\Delta J, R), \quad (7)$$

where:

ΔJ = contour integral for cyclic loading, analogous to the J integral for monotonic loading.

However, Equation (7), as stated in (2.2.1), is only valid when no excessive plasticity exists.

➤ *Stages of fatigue crack propagation and lifetime*

Figure 6 illustrates the typical appearance of the section of an element that has failed due to fatigue. The crack starts around a stress-concentrator point, in this case in a geometrical discontinuity (the keyway), from where it extends gradually forming scratches called "beach marks". During the progressive fracture of material, friction occurs between the faces of the section, producing a smooth and shiny surface.

Finally, the element fails suddenly leaving a rough surface as if it were a fragile material.

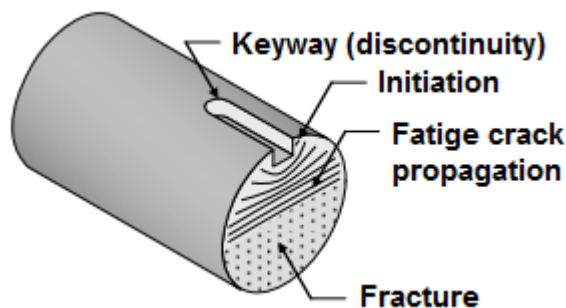


Figure 6-Typical fatigue fracture appearance.

Generally, the lifetime of cyclically loaded structures made of technical alloys consists of three periods: fatigue crack initiation, fatigue crack propagation and final fracture. The crack initiation period is defined as the time or number of loading cycles up to the first detectable crack. However, with respect to the physical damage process, this initiation period can be subdivided into three distinct stages: crack nucleation, short crack regime and long crack regime. Consequently, the complete lifecycle of a fatigue crack, from its nucleation to component failure, passes through the stages shown in Figure 7.

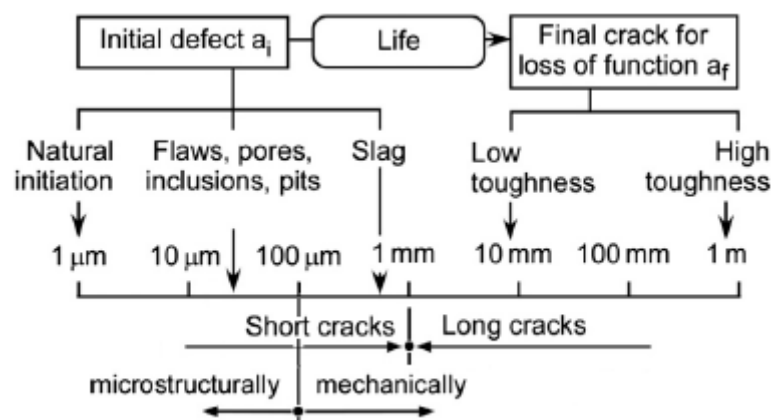


Figure 7-Stages of the lifecycle of a fatigue crack. [11]

○ 1- Crack nucleation

Crack initiation (or nucleation) in a narrower sense is the range within which a crack first develops due to the accumulation of irreversible plastic deformation. This can happen at pre-existing defects which act as stress concentrators due to stiffness mismatch with the matrix material and/or micro notch effects (Figure 8) or – in rare cases

– at the defect free surface. The definition of the end of the initiation phase is a bit academic because it is hard to define when exactly an original defect has become a crack. The concepts of fracture mechanics similitude and a ΔK threshold break down near the point of crack initiation.

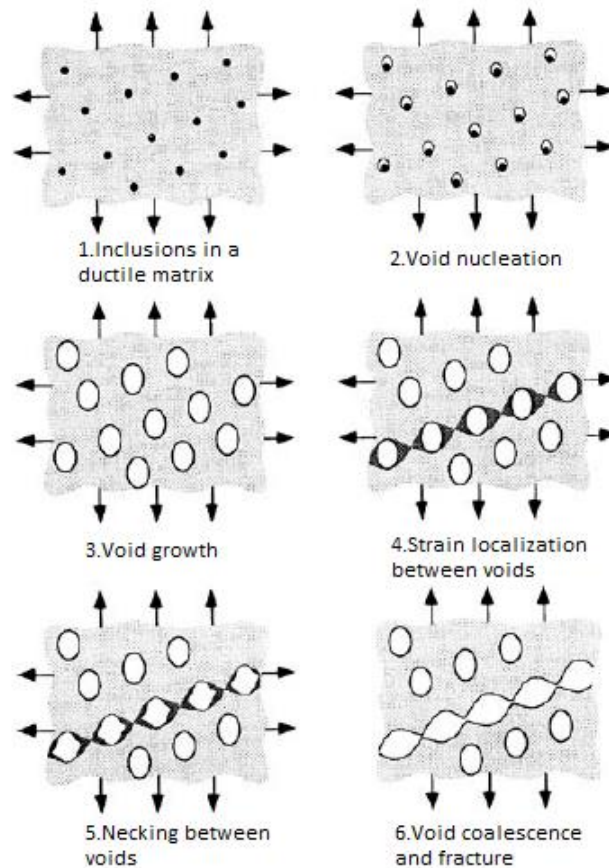


Figure 8-Crack nucleation from inclusions. [2]

Thus, the mechanism for crack nucleation depends on several factors:

- **Material:** Yield limit and microstructure (for example, grain size and orientation, presence of inclusions...).
- **Geometry:** any discontinuity in the mechanic component will be translated into a stress concentrator (for example, a change of section).
- **Surface:** the rougher or irregular its surface, the stronger the concentration of stresses that it induces. Also, the importance of surface treatments (treatments that provide residual stresses of compression are worth against fatigue crack nucleation) must be pointed.
- **Size:** the greater the size of the component, the more probably a microstructural defect exists.
- **Environment:** the aggression of the medium on the surface of the material (corrosion) generates stress concentrators.

○ 2- Crack propagation

➔ *Short Crack Regime*

The short crack regime corresponds to the transition from crack nucleation regime to the long crack regime where fracture mechanics similitude applies. The fatigue behavior of short cracks is often very different from that of longer cracks. There is not a precise definition of what constitutes a "short" crack, but most experts consider cracks less than 1 mm deep to be small. Because most fatigue cracks spend the vast majority of their lives as short cracks, the behavior of such flaws is of significant practical importance.

It is necessary to differentiate between two types of short cracks:

❖ *Microstructurally short cracks*

A microstructurally short crack has dimensions that are on the order of the grain size. Cracks less than 100 μm long are generally considered microstructurally short. The material no longer behaves as a homogeneous isotropic continuum at such length scales; the growth is strongly influenced by microstructural features in such cases. The growth of microstructurally short cracks is often very sporadic; the crack may grow rapidly at certain intervals, and then virtually arrest when it encounters barriers such as grain boundaries and second-phase particles as can be shown on Graph 3.

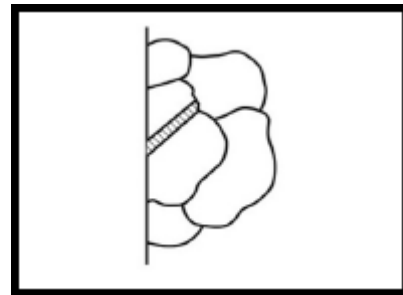
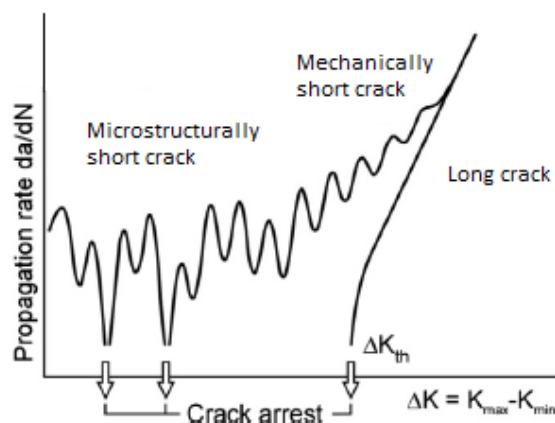


Figure 9-Microstructurally short crack. [11]



Graph 3-Crack propagation stages including the thresholds of fatigue. [11]

❖ *Mechanically short cracks*

A crack that is between 100 μm and 1 mm in depth is mechanically short. The size is sufficient to apply continuum theory, but the mechanical behavior is not the same as in longer cracks. Mechanically short cracks typically grow much faster than long cracks at the same ΔK level, particularly near the threshold.

Two factors have been identified as contributing to faster growth of short cracks: plastic zone size and crack closure.

When the plastic zone size is significant compared to the crack length, an elastic singularity does not exist at the crack tip, and K is invalid. The effective driving force can be estimated by adding an Irwin plastic zone correction.

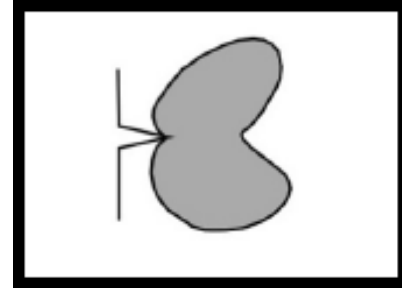


Figure 10-Mechanically short crack. [11]

Application of fracture mechanics to short-crack propagation:

The linear elastic ΔK concept cannot be applied to short cracks since the plastic zone size is in the same order of magnitude as the crack length or – in other words – the crack is even embedded in the plastic zone. As an alternative, elastic-plastic concepts such as the cyclic J integral ΔJ or a cyclic Crack Tip Opening Displacement $\Delta CTOD$ can be used.

→ Long Crack Regime

Eventually a crack which has not been arrested before becomes a long one. The transition is defined by the fully developed crack closure effects, i.e., the stress or K -factor in the loading cycle above which the crack is open has reached a constant value. At that stage crack propagation can be described by the $\frac{da}{dN}$ vs ΔK diagram, however, corrected for the crack closure effects, until the maximum load in terms of the stress intensity factor, K_{max} , is so high that it causes interspersed events of monotonic crack extension.

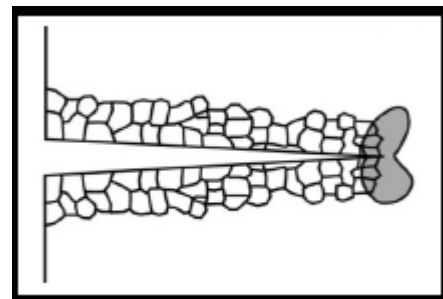


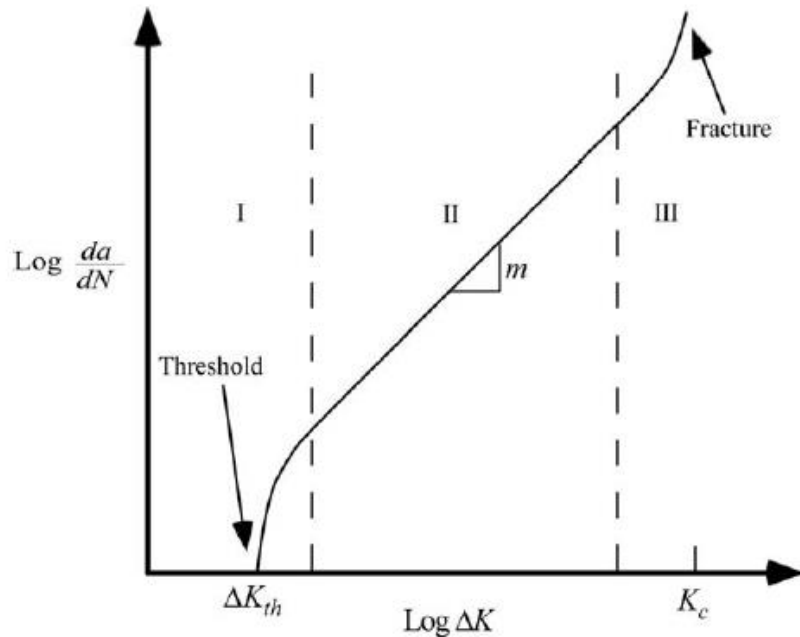
Figure 11-Long crack. [11]

Application of fracture mechanics to long-crack propagation:

- The $\frac{da}{dN}$ vs ΔK diagram

The backbone of fracture mechanics description of long crack propagation is the log-log plot of $\frac{da}{dN}$ vs ΔK . The sigmoidal curve (Graph 4) contains three distinct regions: the threshold region (I), the so-called Paris region (II) and the region where fatigue propagation moves towards fracture (III).

At intermediate ΔK values, the curve is linear, but the crack growth rate deviates from the linear trend at high and low ΔK levels. At the low end, $\frac{da}{dN}$ approaches zero at a threshold ΔK_{th} , below which the crack will not grow.



Graph 4-Typical (long) fatigue crack growth behavior in metals. [9]

The linear region of the log-log plot in Graph 3 can be described by a power law (Paris-Erdogan equation):

$$\frac{da}{dN} = C \Delta K^m, \quad (8)$$

where C and m are material constants that are determined experimentally.

According to equation (8), the fatigue crack growth rate depends only on ΔK ; $\frac{da}{dN}$ is insensitive to the R -ratio in Region II.

Equation (8) has become widely known as the *Paris Law*.

Generally, to simplify the calculations, regions I and III are often disregarded and estimated life to fatigue is done by using exclusively the law of region II. Under this assumption, integrating the Paris equation (8), it results the number of cycles required to propagate a crack from initial length a_o to a final length a_f :

$$N = \int_{a_o}^{a_f} \frac{da}{C \Delta K^m} \quad (9)$$

- The fatigue threshold

The fatigue threshold ΔK_{th} is the point below which a fatigue crack will not grow. Experimental measurements of the threshold are usually inferred from a load-shedding procedure, where ΔK , is gradually reduced (K-decreasing method according to ASTM E647 [12]) until the crack growth rate reaches a very small value. In most experiments in the threshold range, either K_{max} or the R -ratio is held constant, while ΔK is reduced.

- 3- Final failure

The type of fracture produced by fatigue is called commonly *progressive*, due to the gradual way it occurs, *fragile*, because the fracture occurs without appreciable plastic deformation, and *sudden*, because the final failure occurs very quickly.

Failure of the component occurs when the crack reaches its critical state. This can be defined by K_{max} or K_{Ic} (or its elastic-plastic equivalent) exceeding the monotonic fracture resistance of the material but also by other characteristics which cause the loss of function of the component. Note that the exact definition of the failure criterion, in many cases, is of minor relevance since the crack propagation is very rapid at this stage and there is no much difference in terms of residual lifetime between different definitions.

Comparing the different stages of crack propagation, it is frequently found that neither crack nucleation nor long crack propagation, but the short crack regime decisively contributes to the overall lifetime of the component.

2.3.2.2 Wöhler's curves approach

The oldest approach. It is suitable for HCF regimes.

They are based on Wöhler's curves obtained from testing actual components, and they are preferred for fatigue life prediction of structural members subject to load controlled conditions, where the nominal stresses are the reference magnitude. Its suitability is restricted to the long-life region, i.e., to the elastic stress domain

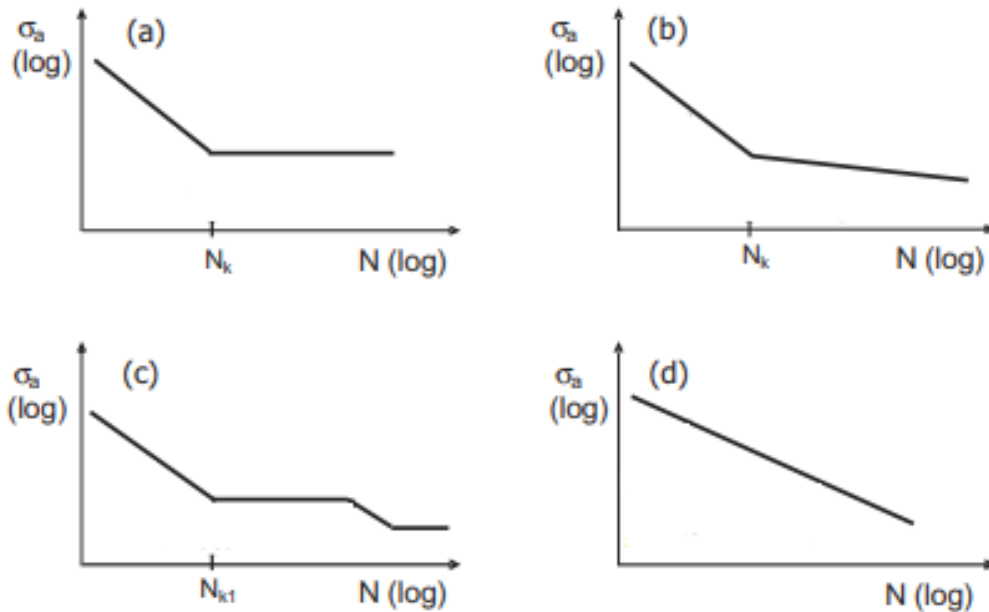
➤ Stress-Number of Cycles curves

In high-cycle fatigue situations, materials performance is commonly characterized by an $S-N$ curve, also known as a Wöhler's curve. This is a graph of the magnitude of a cyclic stress (S) against the logarithmic scale of cycles to failure (N).

In the design codes, the fatigue Wöhler's – or $S-N$ – curves have been proposed to describe the materials and structural details fatigue behavior

$S-N$ curves are derived from tests on samples (called coupons) of the material to be characterized where a regular sinusoidal stress is applied by a testing machine which also counts the number of cycles to failure. This process is sometimes known as coupon testing. Each coupon test generates a point on the plot though in some cases there is a "runout" where the time to failure exceeds that available for the test.

The progression of the $S-N$ curve can be influenced by many factors such as stress ratio (mean stress), loading frequency, material, temperature, corrosion, residual stresses, and the presence of notches. Graph 5 is an example of this dependence.



Graph 5-Typical $S-N$ curves including the VHCF-region: (a) low strength steels, components with sharp notches (b) materials with body-centered cubic lattice under corrosive media or at elevated temperatures, materials with face-centered cubic lattice (c) some high strength steels, components with surface treatment (d) high and very high strength steels, materials with face-centered cubic lattice. [13]

The $S-N$ curves originally proposed by Basquin and adopted in the design codes, is given by following expression:

$$\Delta\sigma \cdot N^m = C, \quad (10)$$

where C and m are material constants. The mean $S-N$ curves may be described by a linear regression analysis using the following linear model:

$$Y = A + B \cdot X, \quad (11)$$

where Y is the dependent variable defined as $\log(N_f)$, X is the independent variable defined as $\log(\Delta\sigma)$, A and B are linear regression parameters. Equation (11) can be rewritten in the following alternative forms:

$$\begin{cases} \log(N_f) = A + B \cdot \log(\Delta\sigma) \\ \log(\Delta\sigma) = -\frac{A}{B} + \frac{1}{B} \cdot \log(N_f) \end{cases} \quad (12)$$

where A and B are linear regression parameters related with the C and m constants:

$$\begin{cases} C = 10^A \\ m = -B \end{cases} \quad (13)$$

➤ *Statistical description of fatigue test*

The direct consequence of the previously-explained mechanism of nucleation is that the fatigue behavior of materials is random in nature and should be studied through statistical laws. That is, two identical specimens tested under one stress amplitude does not break for the same number of cycles. Logically, the nucleation process is random depending on the disorientation between adjacent grains and the presence of stress concentrators. Because of this, the $S-N$ curve should more properly be a Stress-Cycle-

Probability ($S-N-P$) to describe the $S-N$ field as percentile curves, i.e. curves representing constant probabilities of failure that are represented by equilateral hyperbolas (see Graph 6).

Probability distributions that are common in data analysis and in design against fatigue include the Weibull, Gumbel and Fréchet distributions for minima or for maxima, which represent the so-called attraction domains for whatever distribution. Physical considerations of the phenomenon handled allow the characteristic of minima of maxima distribution exhibited by the reference variable to be unequivocally discerned. In fatigue, both reference variables namely lifetime, i.e. number of cycles, and stress evidence a problem related to minima. By the way, the Fréchet distribution for minima must be discarded since it exhibits no lower bound but a limiting upper bound of the lifetime thus contradicting physical evidences in the fatigue phenomenon. Accordingly, only the Weibull distribution is eligible or, possibly, the Gumbel one.

Three models are used in literature for description of S-N curve:

- The Basquin's model

Often, the Wöhler-curve is represented as a straight line in a double logarithmic plot. Therefore, it is judicious to model the Wöhler's curve by Basquin's equation. Thus, material parameters (A , B) of Basquin's equation are given in following equation:

$$\sigma = AN^B. \quad (14)$$

It is noted that, the dispersion results from the same level of loading is already observed. Such a phenomenon is due to several factors, such as material defects during the process of extrusion and the machining process of specimens etc.

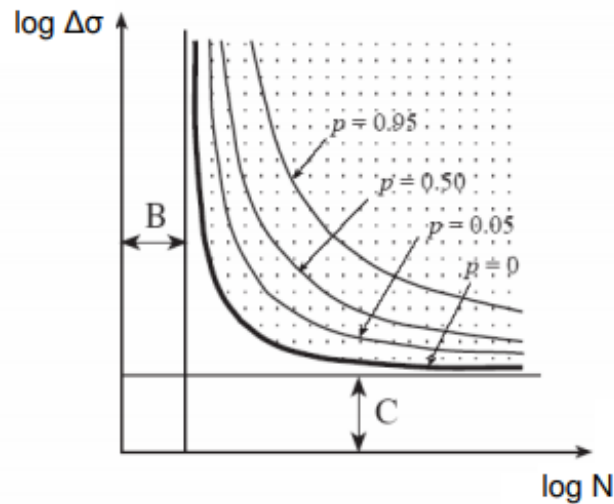
- The Canteli-Castillo model

Castillo and Fernández-Canteli proposed a model based on a three parameter Weibull model for the analysis of fatigue results able to consider specimens with different lengths: The solution of the model for the S-N field considering an element of length L_i subject to a constant amplitude loading $\Delta\sigma$, is given by:

$$(\log N - B)(\log \Delta\sigma - C) = D \left[\left(-\frac{L_0}{L_i} \log(1 - P) \right)^{1/A} - E \right], \quad (15)$$

where N is the fatigue life measured in cycles, $\Delta\sigma$ is the stress range, $P = f(\log N; \Delta\sigma)$ is the probability of failure, L_0 is the reference length, L_i is the specimen length and A , B , C , D , and E are the model parameters to be estimated with the following meaning:

- A: Shape parameter of the Weibull distribution.
- B: Threshold value of N or limit number of cycles.
- C: Threshold value for $\Delta\sigma$ or endurance limit.
- D: Scale factor.
- E: Parameter defining the position of the limit curve or zero probability curve.



Graph 6-S-N field with percentile curves representing the same probability of failure. [14]

The estimation of the parameters follows in two steps. In the first step B and C are estimated while the rest of the parameters, i.e., A, D and E are calculated in a second stage. Different mathematical methods have been proposed by Castillo et al. [15], [16], [17].

- The Kohout-Věchet model

In 2.3.1, it was said that typical civil-engineering structures, were usually designed for high-cycle fatigue (HCF). Recently, several failures of these structures cannot be explained only with the HCF regime taking into account the extreme loading conditions to which the structural elements are subject (e.g. earthquakes). Recent studies suggest the use of S-N curves considering both LCF and HCF regimes [18], [19]. The full-range S-N curve based on stress damage parameter, proposed by Kohout and Věchet has been increasingly used in the fatigue life evaluation of existing bridges structures because this model covers all fatigue regimes, LCF and HCF regimes, that is, this model describes the region of cycles from tensile strength to permanent fatigue limit (Graph 7).

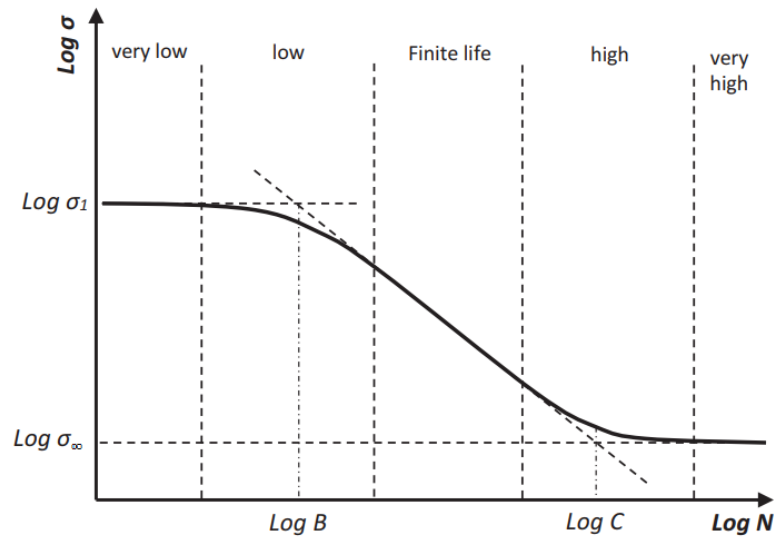
The KV fatigue model is expressed by the following relation:

$$\sigma(N) = a \left[\frac{(N+B)C}{N+C} \right]^b \equiv \sigma_{\infty} \left(\frac{N+B}{N+C} \right)^b \equiv \sigma_1 \left(\frac{1+N/B}{1+N/C} \right)^b, \quad (16)$$

where a and b are the Basquin parameters, σ_{∞} is the fatigue limit, σ_1 is the ultimate tensile strength, B is the number of cycles corresponding to the intersection of the tangent line of the finite life region and the horizontal asymptote of the ultimate tensile strength, and C is the number of cycles corresponding to the intersection of the tangent line of the finite life region and the horizontal asymptote of the fatigue limit. B and C parameters are given by:

$$B = \beta \cdot C \quad (17)$$

$$C = 10^7 \frac{1-\gamma}{\gamma-\beta} \quad (18)$$



Graph 7-Schematic representation of the Kohout-Věchet S-N curve. [20]

2.3.3 The Compact Test specimen (ASTM E647)

Regarding the American Society for Testing and Materials (ASTM), the compact tension specimen, CT, is a single edge-notch specimen loaded in tension. The CT specimen has the advantage over many other specimen types in that it requires the least amount of test material to evaluate crack growth behavior.

Fracture mechanics theory applies to cracks that are infinitely sharp prior to loading, therefore a machined notch is done in the specimen, to facilitate fatigue precracking. It may be made by electrical-discharge machining (EDM), milling, broaching, or sawcutting.

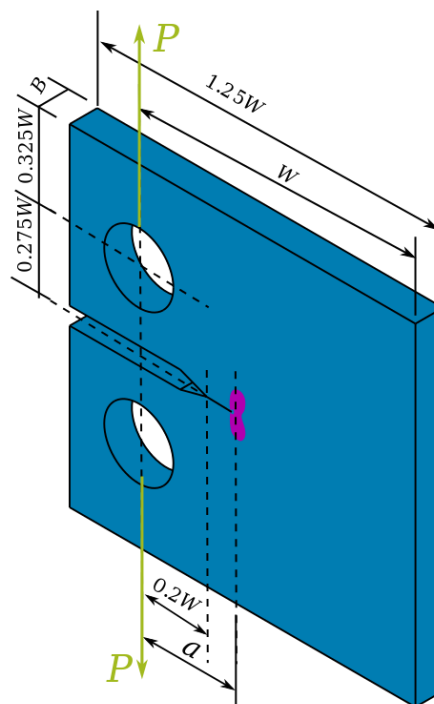


Figure 12-Typical CT specimen [21].

2.3.3.1 Specimen geometry and dimensions

The thickness, B , and width, W , may be varied independently within the following limits, which are based on specimen buckling and through-thickness crack-curvature considerations: For CT specimens it is recommended that thickness be within the range $W/20 \leq B \leq W/4$.

For results to be valid according to this test method it is required that the specimen be predominantly elastic at all values of applied force. For the CT specimen the following is required:

$$(W - a) \geq (4/\pi)(K_{max}/\sigma_{YS}), \quad (19)$$

where:

$(W - a)$ = specimen's uncracked ligament and

σ_{YS} = 0.2 % offset yield strength determined at the same temperature as used when measuring the fatigue crack growth rate data.

Also, because we are modelling in 2D in plane strain conditions, it is required that both the specimen thickness, B , and the crack length, a , exceed $2.5 \left(\frac{K_{Ic}}{\sigma_{ys}} \right)^2$.

The crack length, a (crack starter notch plus fatigue crack) is nominally equal to the thickness, B , and is between 0.45 and 0.55 times the width, W . The ratio W/B is nominally equal to two.

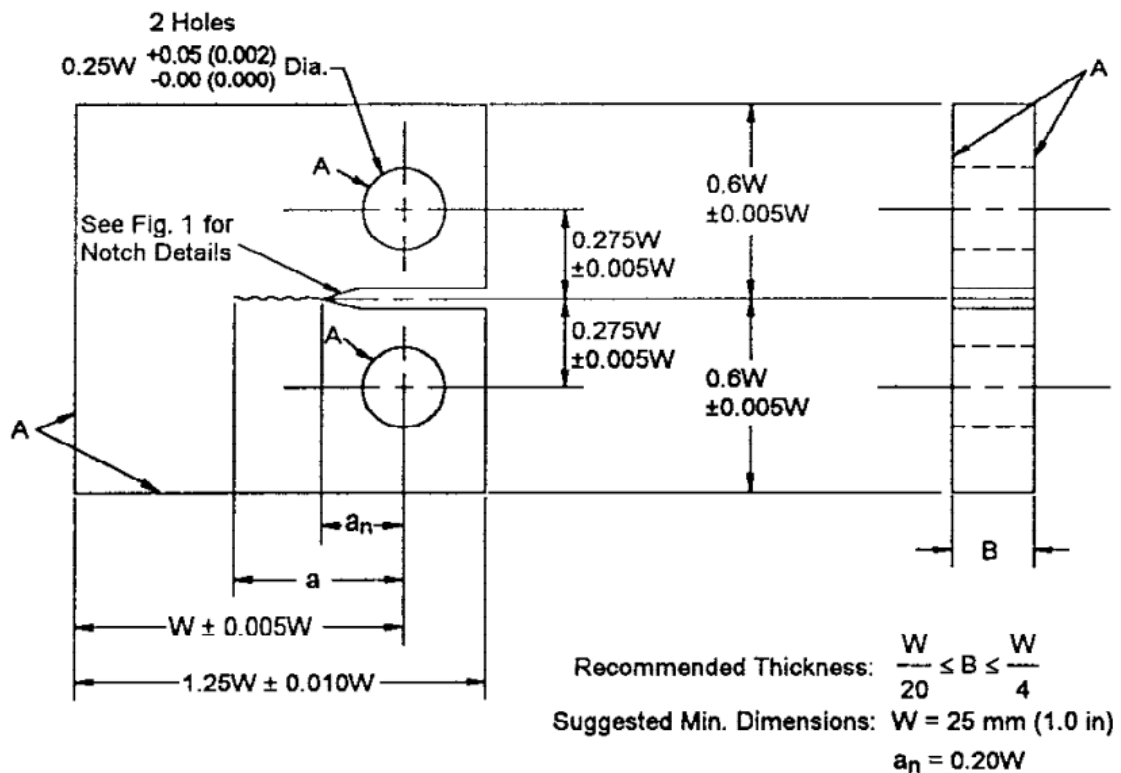


Figure 13-CT dimensions. [22]

A clevis-and-pin assembly is used at both the top and bottom of the specimen to allow in-plane rotation as the specimen is loaded. This specimen and loading arrangement is to be used for tension-tension loading only, as illustrated in Figure 14.

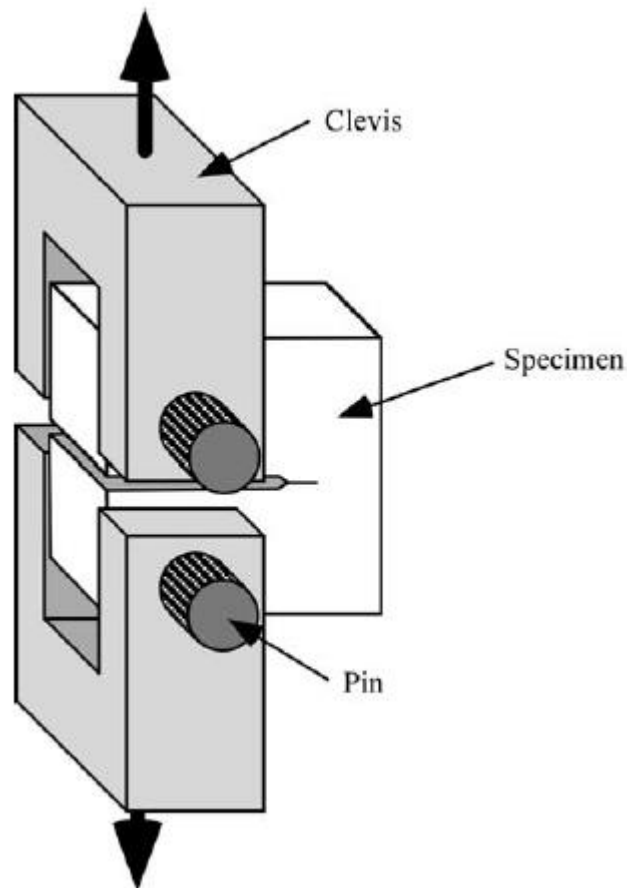


Figure 14-Apparatus for testing CT specimens. [9]

2.3.4 Structural steel S355 (EN 10025)

Structural steel is a standard construction material, made from specific grades of steel and formed in a range of industry standard cross-sectional shapes. Structural steel grades are designed with specific chemical compositions and mechanical properties formulated for particular applications.

In Europe, structural steel must comply with the European Standard EN 10025 and Governed by the ECIS (European Committee for Iron and Steel Standardization) a subset of CEN (European Committee for Standardization).

European standard steel grade names fall into two categories:

1. Steel specified by purpose of use and mechanical properties.
2. Steel specified by chemical composition.

According with those standards, basic grade designations for *category 1* steels consist of a single letter (designating application) then a number signifying the

mechanical property dictated in the standard for that application designation, as can be shown in Table 1:

Application symbol	Meaning	Mechanical Property
S	Structural steel	Minimum Yield Strength
P	Steel for pressure lines and vessels	Minimum Yield Strength
L	Steel for pipe and tube	Minimum Yield Strength
E	Engineering steels	Minimum Yield Strength
B	Steel for reinforced concrete	Characteristic Yield Case
R	Steel for rail use	Minimum Yield Case
H	High Tensile Strength Flat products	Minimum Yield Case
D	Flat Products for Cold Forming	
T	Tinmill Products	Nominal Yield Case
M	Electrical Steel	

Table 1-Basic grade designation for category 1 steels.

In addition to the above category codes there are symbols that can be added to the grade code to identify any additional compositional requirements, delivery conditions, mechanical properties and so on.

Since we are interested only in structural steels, the most common additional symbols for this application are shown in Table 2 and Table 3:

Impact Resistance		Temperature	
Impact code	Testing strength	Temperature code	Testing temperature
J	27 J	R	Room temperature
K	40 J	0	0 °C
L	60 J	2	-20 °C
		3	-30 °C
		4	-40 °C
		5	-50 °C
		6	-60 °C

Table 2-Impact and temperature codes for structural steels, category 1.

Code	Condition
A	Annealed
QT	Quenched and tempered
N	Normalized
SR	Stress relieved
C	Cold worked
U	Untreated

Table 3-Delivery condition codes for structural steels, category 1.

Obviously, the EU Standard classifications are inherently not a global standard and therefore a number of corresponding grades with the same chemical and mechanical properties may be used in other parts of the world. For example, structural steels fabricated for the US market must be specified in accordance with the ASTM (American Society for Testing and Materials).

In this way, S355 is known in the USA as A572Gr50.

The use of S355 high strength steel in civil engineering to design bridges, its elements or simple engineering parts allows material and economical savings meeting the strict construction requirements.

Chemical composition of structural steel is extremely important and highly regulated. It is a fundamental factor which defines the Mechanical properties of the steel material.

Grade	C%	Mn%	P%	S%	Si%
S355	0.23 max	1.60 max	0.05 max	0.05 max	0.05 max

Table 4-Chemical composition of S355.

Mechanical properties of structural steel are fundamental to its classification and hence, application.

The **Yield strength** (σ_Y) of structural steel is the stress the material can withstand without permanent deformation. This is not a sharply defined point. Yield strength is the stress which will cause a permanent deformation of 0.2% of the original dimension.

As said before, S355 is named based on its minimum yield strength of 355 MPa, however the yield strength reduces when the thickness is increased above 16 mm for flat products and hollow sections, as can be shown in Table 5:

Thickness, t [mm]	Yield Strength [MPa]
Up to 16	355
16 < t ≤ 40	345
40 < t ≤ 63	335
63 < t ≤ 80	325
80 < t ≤ 100	315
100 < t ≤ 150	295

Table 5-Yield Strength for S355.

The **Ultimate Tensile Strength (UTS)** of Structural steel relates to the point of maximum stress that the material can withstand.

S355 ultimate tensile strength ranges also varies based on thickness, as shown in Table 6:

Thickness, t [mm]	Tensile Strength [MPa]
Up to 3	510 to 680
3 < t ≤ 100	470 to 630
100 < t ≤ 150	450 to 600

Table 6-Ultimate strength for S355.

The **Density (ρ)** of S355 is 7850 kg/m³ like all other mild steel.

Therefore, all the above-mentioned properties vary depending on the grade of the S355 steel and in the thickness. In this thesis, two different grades will be evaluated:

- S355 J2: Testing strength of 27J at a temperature of -20 °C.

Steel grade	C max. %	Mn max. %	Si max. %	P max. %	S max. %	N max. %	Cu max. %	Other max. %
S355 J2	0,22	1.60	0.55	0,030	0,030	-	0,55	-

Table 7-Chemical composition in percentage by weight of steel grade S355 J2 according to EN 10025-2:2004 standard.

- S355 J0: Testing strength of 27J at room temperature (20 °C).

Steel grade	C max. %	Mn max. %	Si max. %	P max. %	S max. %	N max. %	Cu max. %	Other max. %
S355 J0	0,22	1.60	0.55	0,035	0,035	0.012	0,55	-

Table 8-Chemical composition in percentage by weight of steel grade S355 J0 according to EN 10025-2:2004 standard.

3. AIM OF THESIS

The objective of this thesis is to measure, evaluate and compare fatigue properties of different S355 steels. Fatigue and Fracture Mechanics properties such as SIF and T-stress will be also considered.

To this end, the Finite Element model of compact tension is prepared and the calibration curves are calculated.

The S-N curves of two standard S355 steel grades ("J0" and "J2") are evaluated by Basquin's model and the crack propagation rate curves are evaluated by compact tension specimens. The stress intensity factor and the T -stress in the crack tip are also measured.

Those experimental data from IPM and numerical data obtained from FEM software are evaluated and compared with literature.

4. NUMERICAL MODELING IN ANSYS

Software ANSYS is used to obtain numerically values for the K factor and T -stress. It is recommended to see Appendix 10.5 "APPENDIX V - Macro for the CT specimen" to check the modeling. Further information about the commands used, can be found in [30].

4.1 Prior set up

Prior to start with the modeling in the preprocessor, some adjustments should be done: clean the setup area, set the title of the file, order the numeration of key points, lines and areas, set the coordinate system, clear variables, stablish the color of the elements to be displayed and apply 2D, plane strain conditions.

4.2 Pre-processor

4.2.1 Specimen

Once in the pre-processor, it is time to set the parameters that are going to lead the analysis.

As previously said (2.3.3), the specimen chosen is the CT one. The characteristic dimensions are shown in Figure 13.

Because 2D analysis plane strain is performed, the parameters to be defined, as can be shown, are W and a . W is the specimen width and a is the crack length.

W is set as 50 mm while a depends on the a/W ratio, that is stablished from 0.02 to 0.90 in steps of 0.02.

4.2.2 Element type

The ANSYS element library consists of more than 100 different element formulations or types, as shown in Figure 15.

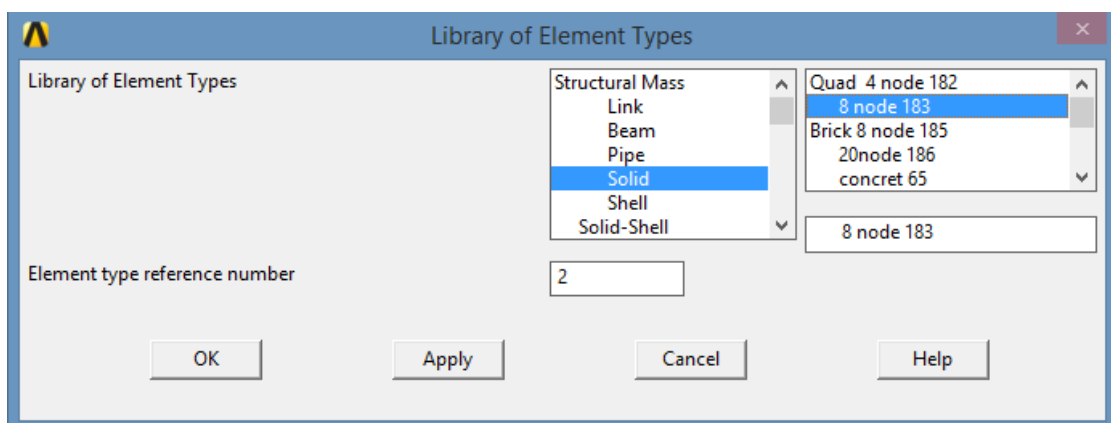


Figure 15-List of some of the element types available in ANSYS.

An element type is identified by a name (8 characters maximum), such as "BEAM3", consisting of a group label (BEAM) and a unique, identifying number (3).

Each element type has a degree of freedom set, which constitute the primary nodal unknowns to be determined by the analysis. They may be displacements, rotations,

temperatures, pressures, voltages, etc. Derived results, such as stresses, heat flows, etc., are computed from these degree of freedom results. Degrees of freedom are not defined on the nodes explicitly by the user, but rather are implied by the element types attached to them. The choice of element types is therefore, an important one in any ANSYS analysis.

For this modeling, element "PLANE82" (in Figure 15, selected as "Solid"> "8 node 183") is chosen because it is required, for the calculation of the stress intensity factor, a shift of one node to 1/4 of the element length.

"PLANE82" provides more accurate results for mixed (quadrilateral-triangular) automatic meshes and can tolerate irregular shapes without as much loss of accuracy. The 8-node elements have compatible displacement shapes and are well suited to model curved boundaries.

The 8-node element is defined by eight nodes having two degrees of freedom at each node: translations in the nodal x and y directions. The element may be used as a plane element or as an axisymmetric element. The element has plasticity, creep, swelling, stress stiffening, large deflection, and large strain capabilities.

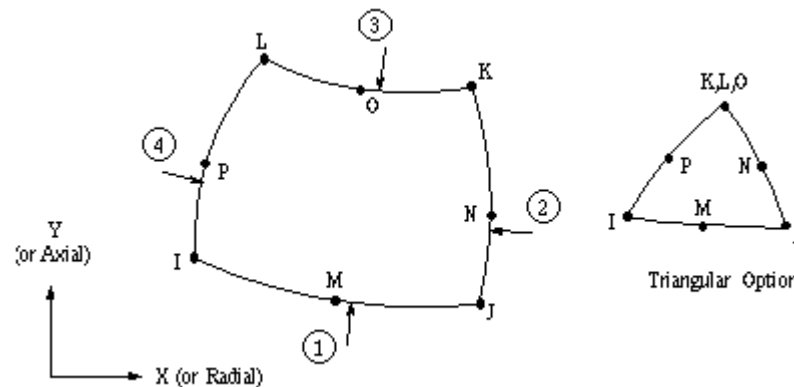


Figure 16-PLANE82, 2-D, 8-Node, Structural Solid. [23]

4.2.3 Material

Various material properties are used for each element type. In this case, all the elements have the same material: S355 steel. Typical material properties include Young's modulus (of elasticity), density, coefficient of thermal expansion, thermal conductivity and so on.

In this case, only the Young's modulus (in MPa) and the Poisson's ratio (dimensionless) are required, as shown in Figure 17.

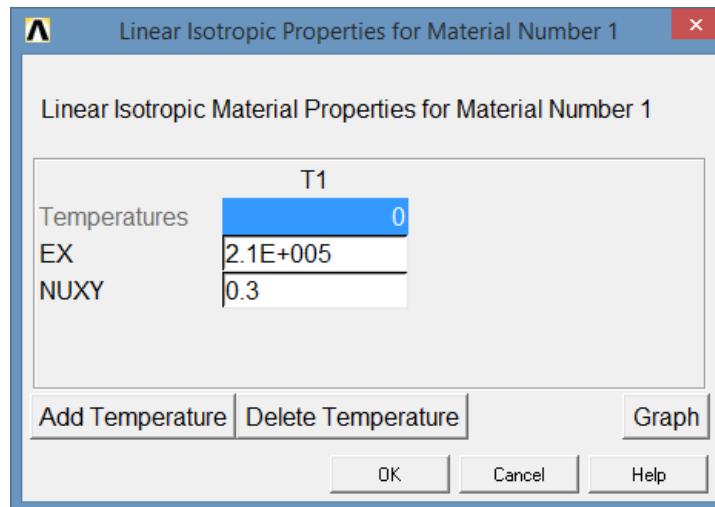


Figure 17-Linear isotropic properties for steel. Young's modulus (EX) [MPa] and Poisson's number (NUXY) [-].

4.2.4 Modelling of the specimen

Symmetry of the specimen (Figure 18) is considered to simplify so that only half of the CT specimen is created (the part above the plane of symmetry).

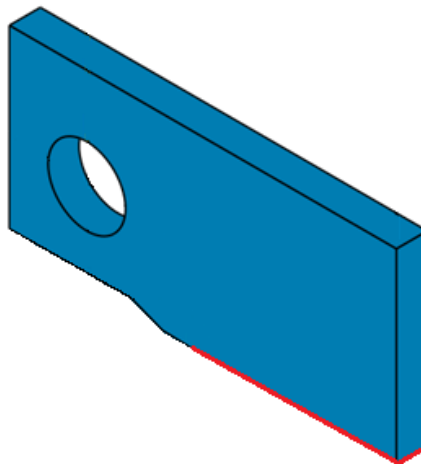


Figure 18-Plane of symmetry (in red) considered.

Notice that the Figure 18 is in 3D only to be clearer. The numerical analysis in ANSYS is performed in 2D, as previously said.

4.2.4.1 Key points

The key points (KP) were defined following this guideline: crack tip is the origin of coordinates and rest of the KP are calculated considering the dimensions pointed in item 2.3.3.

A total of 13 KP are used to create the specimen.



Figure 19-KP of the specimen numerated.

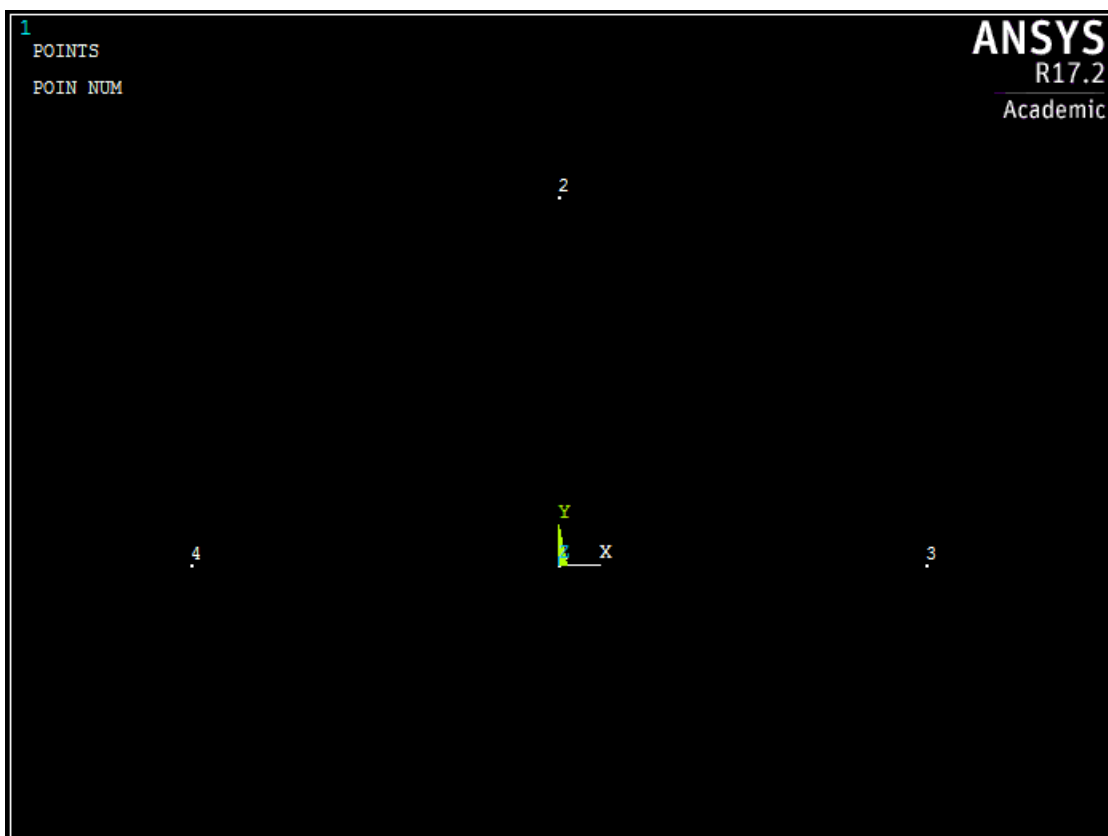


Figure 20-Detailing of the KP at the crack tip.

4.2.4.2 Lines

The KP are joined by straight lines and arcs, as shown in Figure 21.
 A total of 16 lines are used to create the specimen.

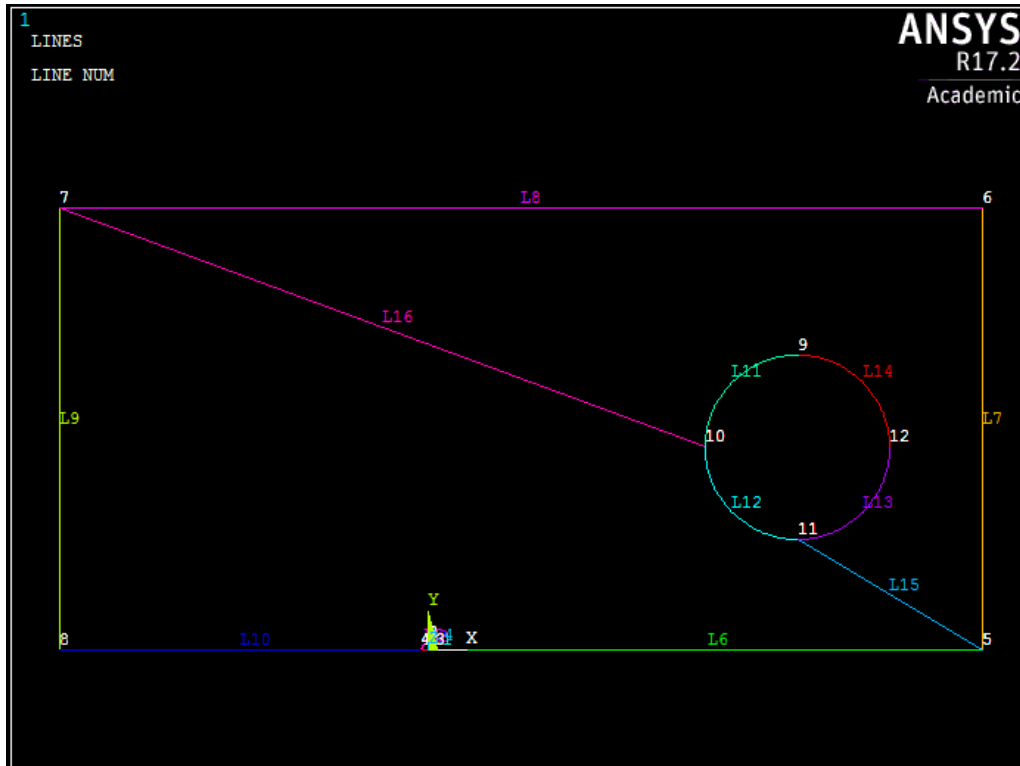


Figure 21-Lines of the specimen numerated.

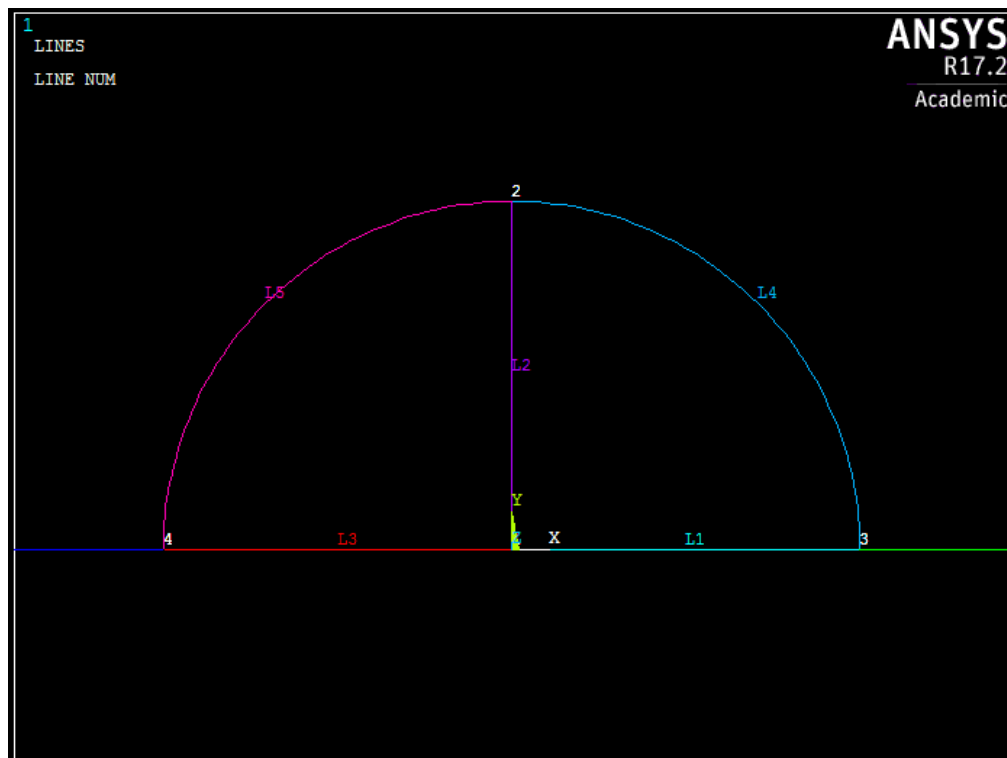


Figure 22-Detailing of the lines at the crack tip.

4.2.4.3 Areas

From the lines previously defined, four different areas are obtained, as shown in Figure 23.

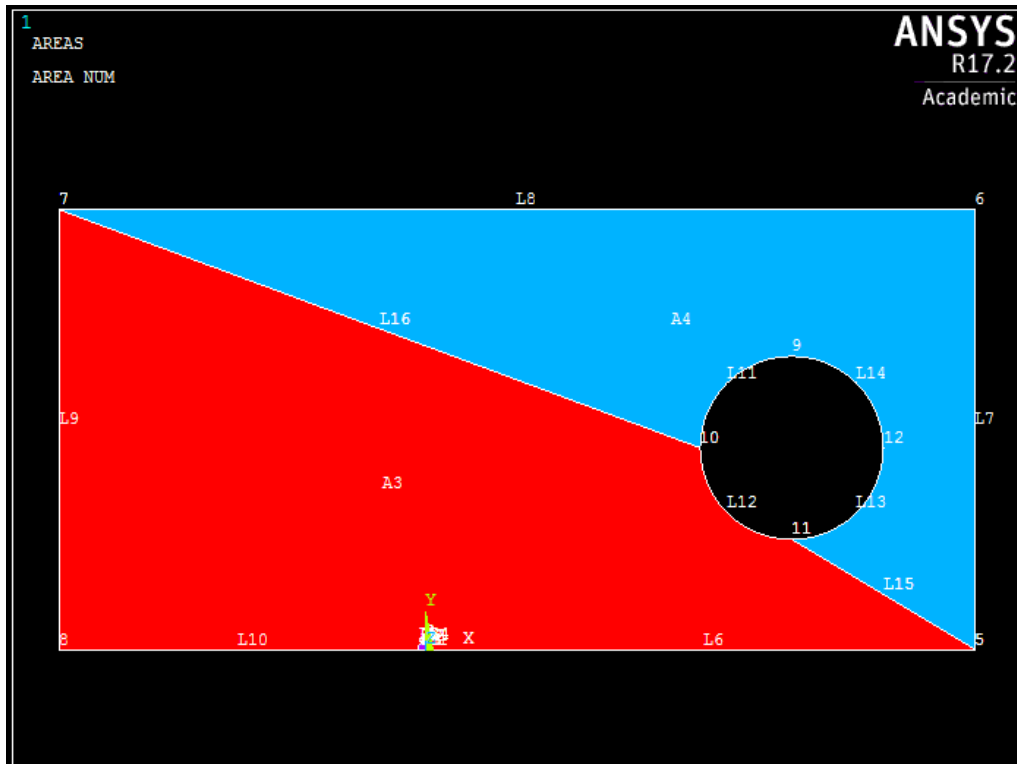


Figure 23-Areas of the specimen numerated.

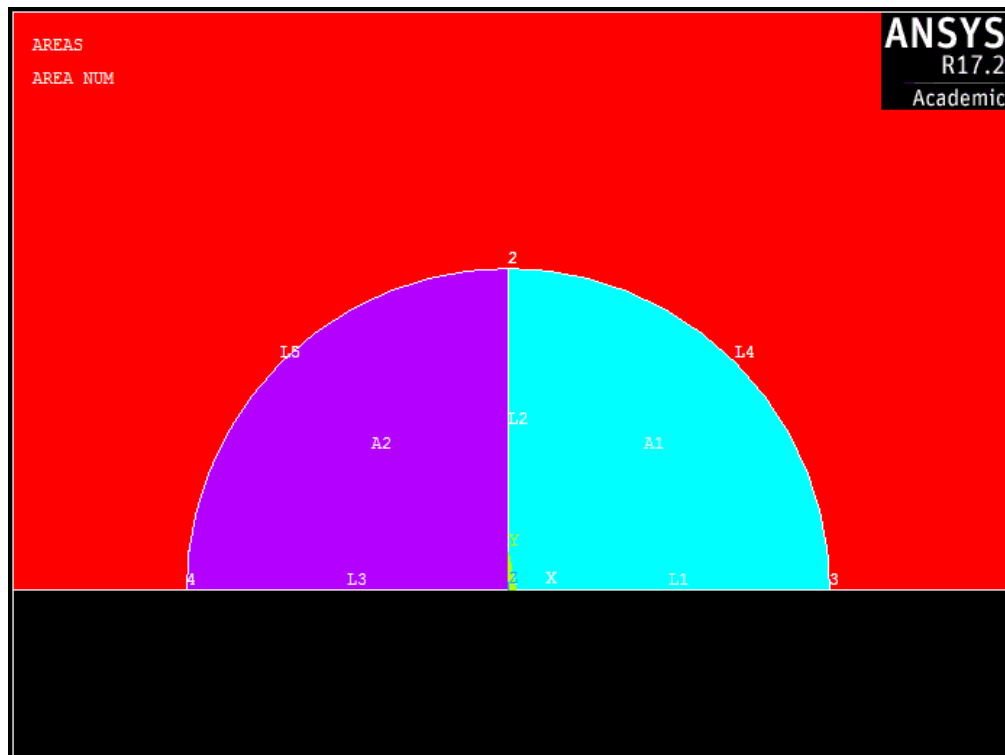


Figure 24-Detailing of the areas at the crack tip.

4.2.5 Meshing

First, the switch of the node in the crack-tip to the $1/4$ point for crack tip singularity is done, allowing to generate focused mesh at the crack tip.

Then, the size of the elements in the mesh is set as follows: 5 mm for elements that are far away the crack tip (due to the less accuracy required) and 1 mm for elements that are near the tip.

Finally, the meshing is performed in all the areas, making the results more accurate, due to the addition of elements.

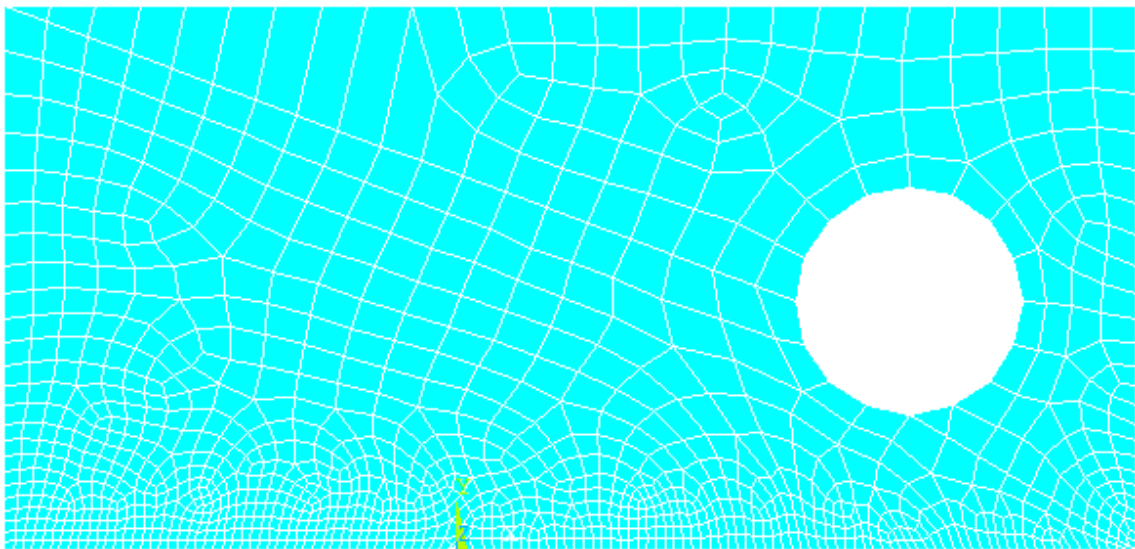


Figure 25-Meshing of the specimen.

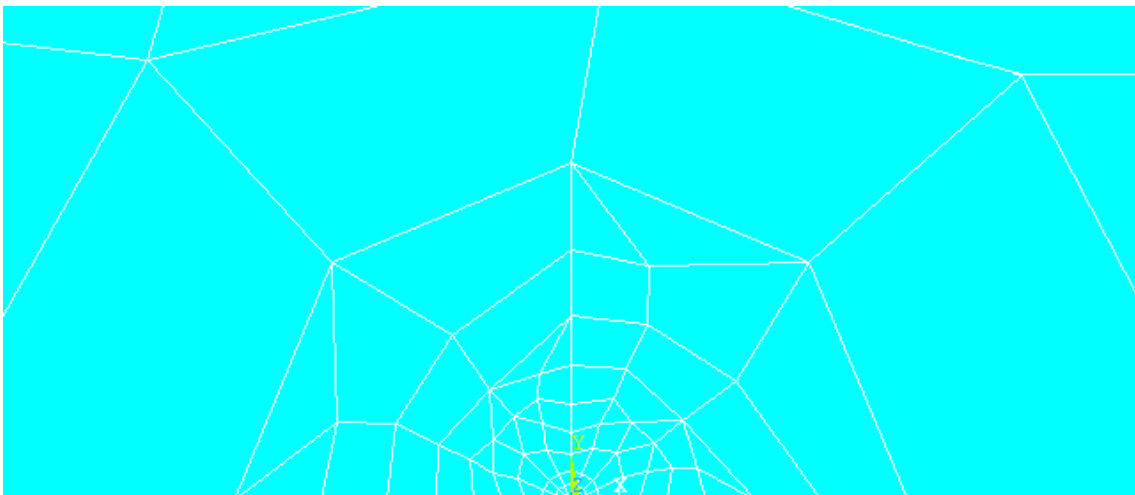


Figure 26-Detailing of the concentrated meshing around the tip.

4.2.6 Boundary conditions

4.2.6.1 Symmetry

It is now when the symmetry is applied, along the X-axis, as pointed previously.

4.2.6.2 Supports

It is needed to locate a support, as can be shown in Figure 27, that is, to restrict the displacement in X-direction, in the point where the load is applied.

4.2.6.3 Loads

A constant load of 1 kN is then applied in the hole of the specimen, also, as shown in Figure 27, in the positive Y-direction.

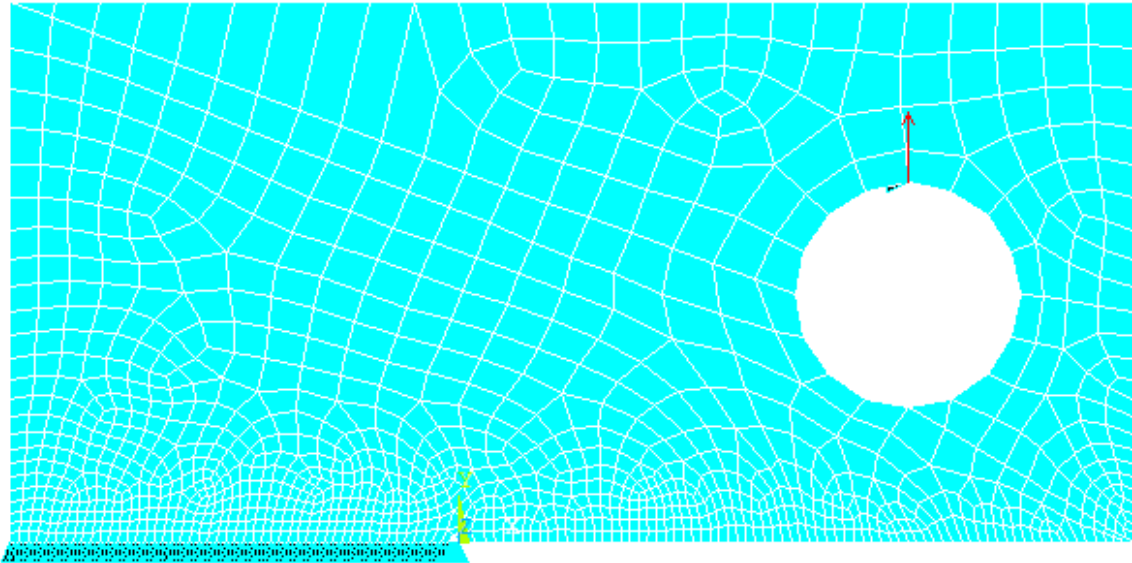


Figure 27-All boundary conditions applied upon the specimen.

4.3 Solve

Once the solution is done, several data can be evaluated. As examples, the stress intensity in the elements around the tip (Figure 28) and the deformation of the specimen (Figure 29) for $a/W=0.5$, are shown.

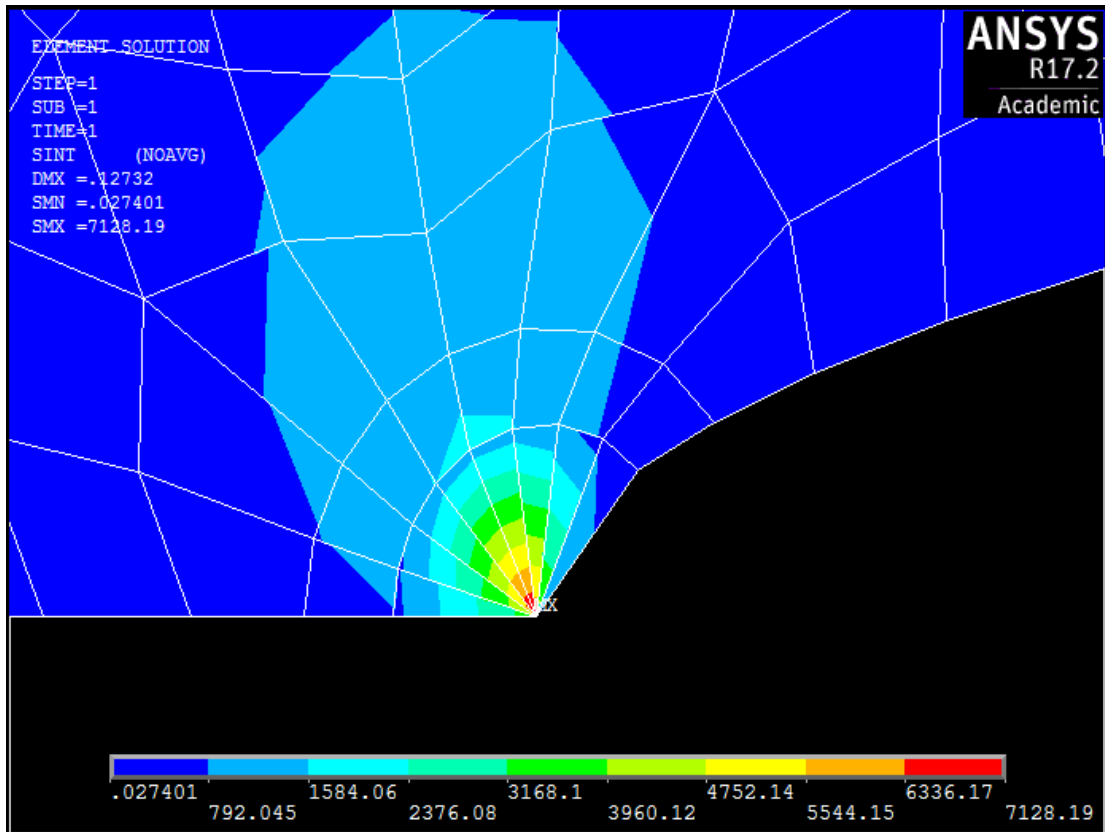


Figure 28-Stress intensity [MPa] around the tip for $a/W=0.5$ and deformed crack tip.

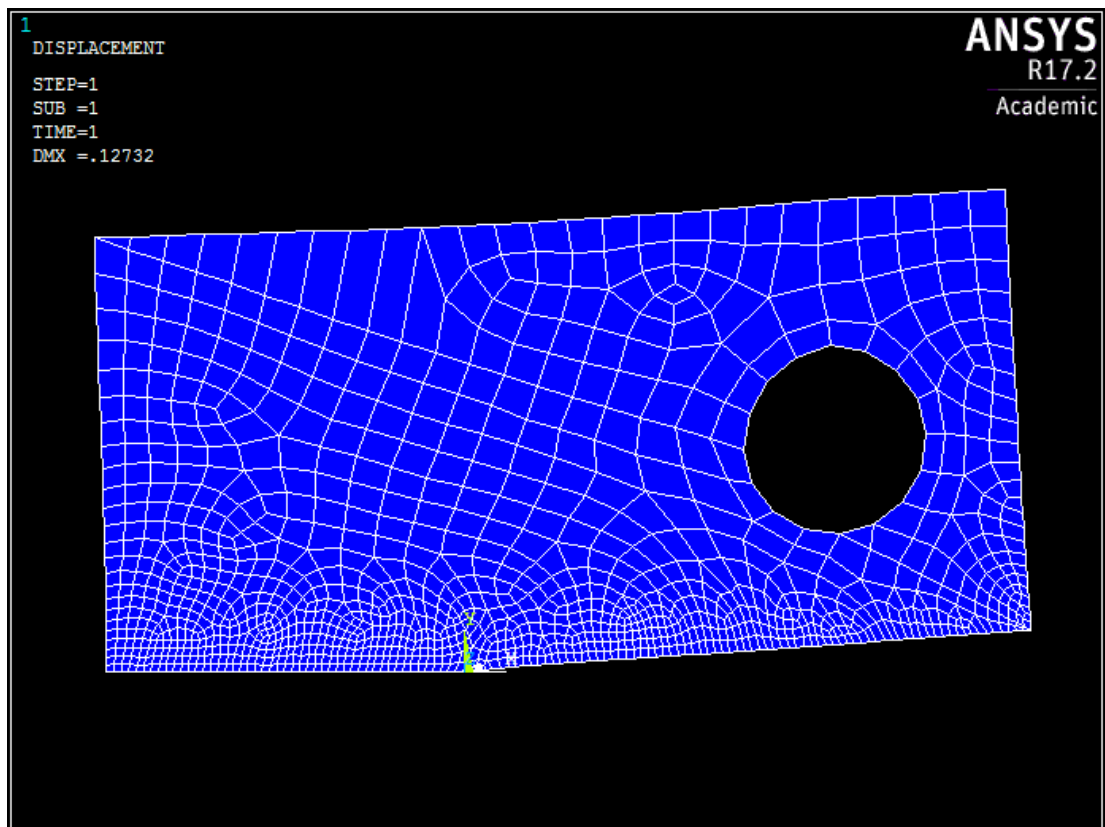


Figure 29-Deformed shape for $a/W=0.5$.

4.4 Post-processor

Once the model is created and solved, it is time to get both the SIF and the T -stress.

4.4.1 Stress Intensity Factor

```

**** CALCULATE MIXED-MODE STRESS INTENSITY FACTORS ****
ASSUME PLANE STRAIN CONDITIONS
ASSUME A HALF-CRACK MODEL WITH SYMMETRY BOUNDARY CONDITIONS (USE 3 NODES)
EXTRAPOLATION PATH IS DEFINED BY NODES:      1      3      4
WITH NODE      1 AS THE CRACK-TIP NODE

USE MATERIAL PROPERTIES FOR MATERIAL NUMBER      1
EX = 0.21000E+06  NUXY = 0.30000  AT TEMP = 0.0000

**** KI = 964.34 , KII = 0.0000 , KIII = 0.0000 ****
    
```

Figure 30-KI calculation in ANSYS for $a/W=0.5$.

As can be shown in Figure 30 (“extrapolation path is defined by nodes 1 3 4 with node 1 as the crack-tip node”), it is necessary to define a path that goes through the crack tip to other two nodes, located in the same line of the tip but in the opposite direction of the crack propagation. This path can be seen in Figure 31.

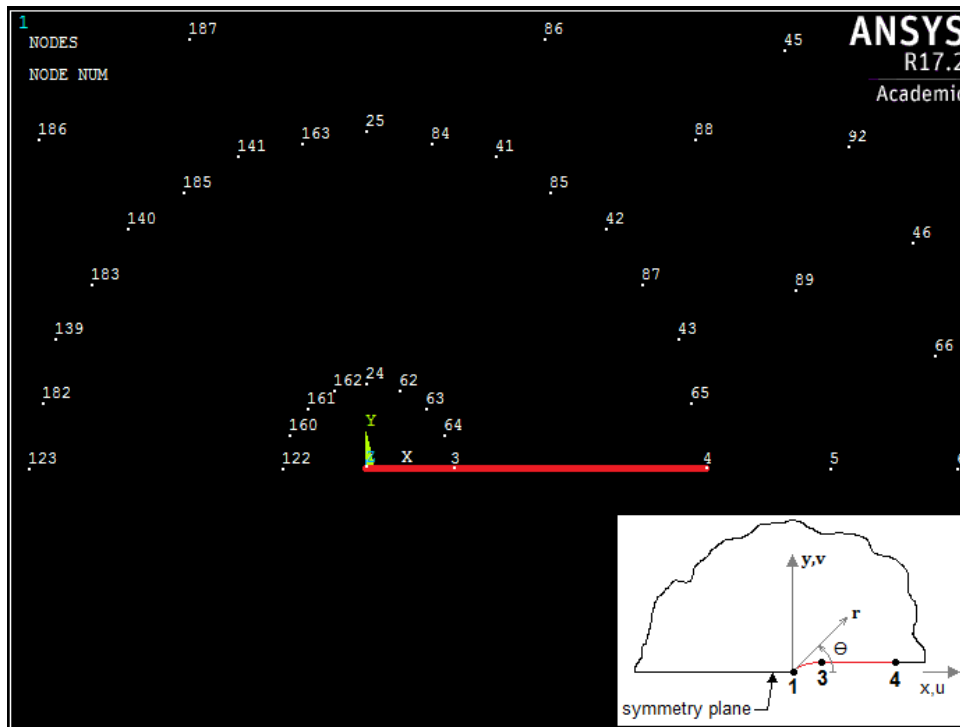


Figure 31-Path established (in red) for the calculation of K_I and schematic representation including Polar and cartesian coordinates for the considered model (half-crack).

4.4.2 *T*-stress

Equation (3) was said to be the method used for the calculation of the *T*-stress, so the aim is to get the stresses σ_{xx} , σ_{yy} with ANSYS and then make the computation to obtain the *T*-stress.

ANSYS interpolates the stress along the path, obtaining, then, average element results across elements.

The values of the stresses are calculated in the nodes contained in 1 mm in front of the crack tip (Figure 32).

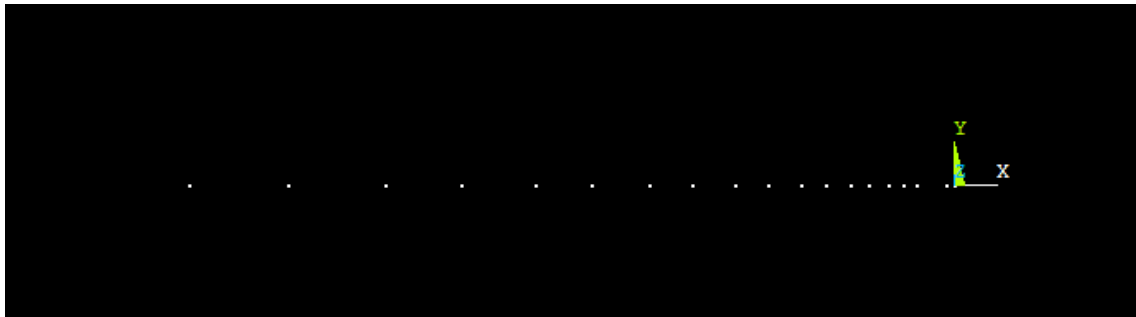


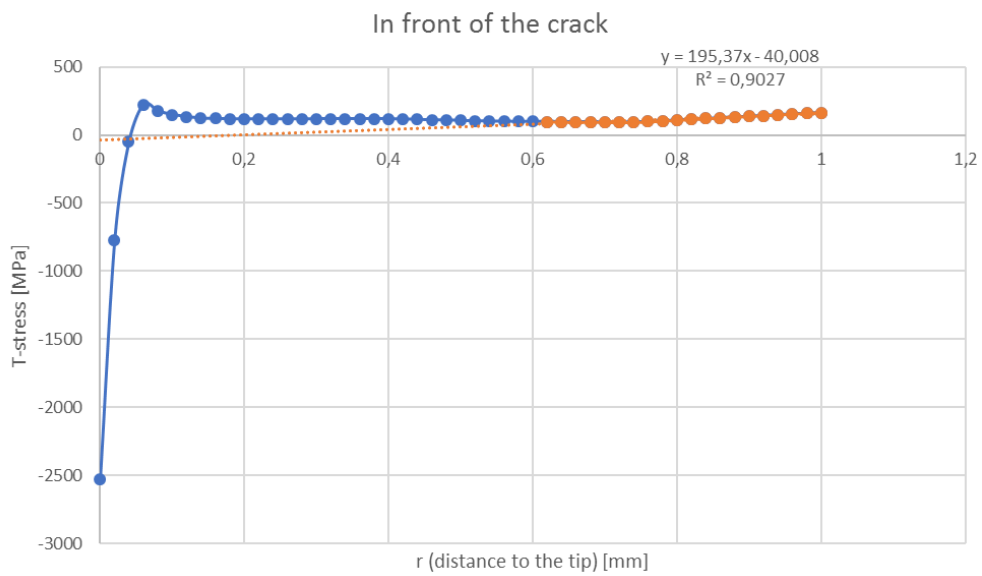
Figure 32-Selection of the nodes in 1 mm in front of the crack tip.

A list, with the distance to the tip (*S*), σ_{xx} (*SX*) and σ_{yy} (*SY*) is generated (Figure 33). The step of the distance *S* is selected depending on the divisions performed in the path.

Then, this list is exported to Excel so that the rest $\sigma_{xx} - \sigma_{yy}$ can be done for each node and a regression is also plotted (Graph 8). Notice that the results of the first nodes (in blue) is depreciated, extrapolating the values only for the -almost ($R^2=0.9027$)- linear part (in orange) from $r=0.6$ mm to $r=1$ mm.

S	SX	SY
0.0000	3756.8	5560.9
0.20000E-01	2308.3	2873.0
0.40000E-01	1708.4	1759.6
0.60000E-01	1436.4	1297.1
0.80000E-01	1375.9	1269.5
0.10000	1285.6	1197.9
0.12000	1177.4	1100.0
0.14000	1077.0	1008.5
0.16000	1018.9	951.80
0.18000	960.69	895.13
0.20000	902.50	838.45
0.22000	868.61	804.57
0.24000	837.16	772.99
0.26000	805.72	741.41
0.28000	774.27	709.82
0.30000	750.13	685.63
0.32000	730.23	665.75
0.34000	710.34	645.86
0.36000	690.44	625.98
0.38000	670.55	606.09
0.40000	650.67	586.23
0.42000	637.81	575.19
0.44000	624.95	564.15

Figure 33-Example of list from ANSYS solution with the distance to the tip (*S*), σ_{xx} (*SX*) and σ_{yy} (*SY*).



Graph 8-Example of regression for the T-stress in front of the crack for $a/W=0.5$.

5. NUMERICAL RESULTS

5.1 Stress Intensity Factors

In the following, several graphs are prepared showing the values of the K_I obtained through:

- ASTM literature calculations.
- Knésl and Bednar literature calculations.
- ANSYS calculations.

5.1.1 ASTM literature calculations

From ASTM [22], the stress intensity factor K_I for the compact tension specimen can be obtained from the following equation:

$$K_I = \frac{P}{B\sqrt{W}} f(\alpha), \quad (20)$$

where:

P is the load applied,

B is the thickness of the specimen,

W is the width of the specimen and

$f(\alpha)$ is a dimensional function that depends on the geometry of the specimens and in ASTM is presented in the following form:

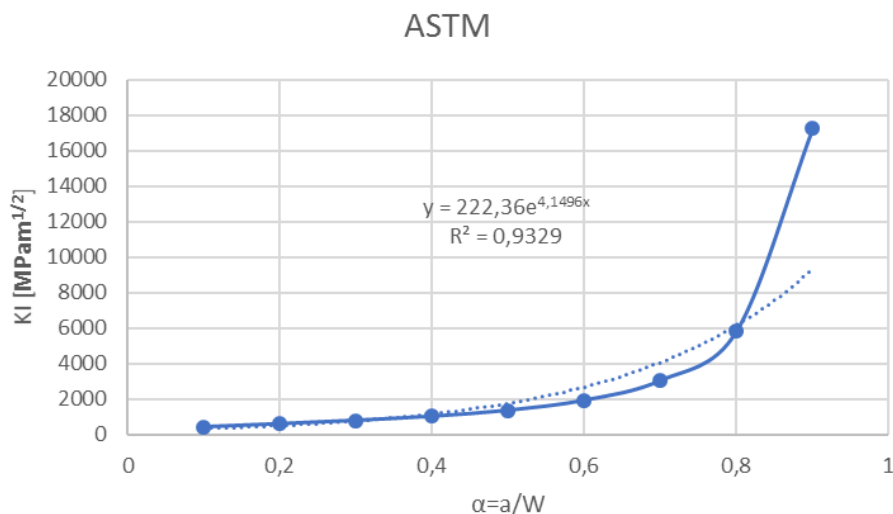
$$f(\alpha) = \frac{(2+\alpha)(0.886+4.64\alpha-13.32\alpha^2+14.72\alpha^3-5.6\alpha^4)}{(1-\alpha)^{3/2}},$$

being

$$\alpha = a/W,$$

where a is the crack size.

In this way, for α values of 0.1 to 0.9 in steps of 0.1:



Graph 9-SIF vs. a/W ratio from ASTM literature calculations [22].

5.1.2 Knésl and Bednar literature calculations

From Knésl and Bednar [24], the stress intensity factor K_I can be obtained as:

$$K_I = K_0 B_1, \quad (21)$$

where:

$$K_0 = \frac{P}{t\sqrt{W}}$$

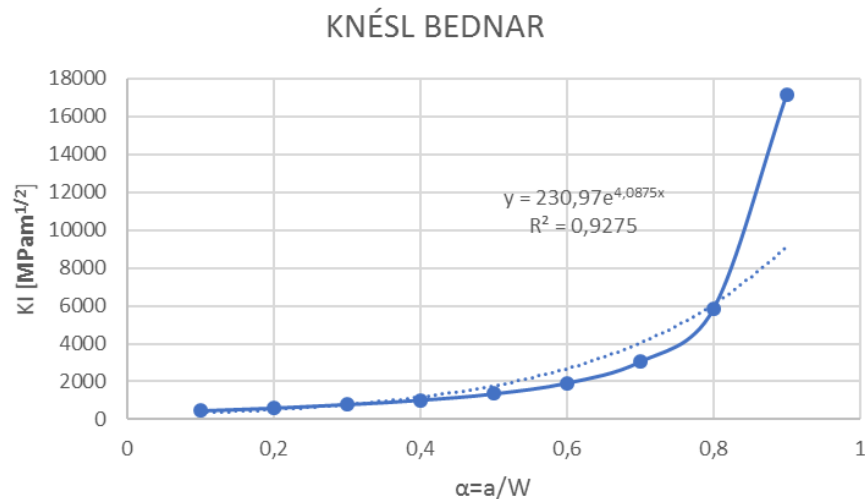
P is the load applied,

t is the thickness of the specimen,

W is the width of the specimen and

B_1 values are given in the literature for each value of the ratio $\alpha = a/W$.

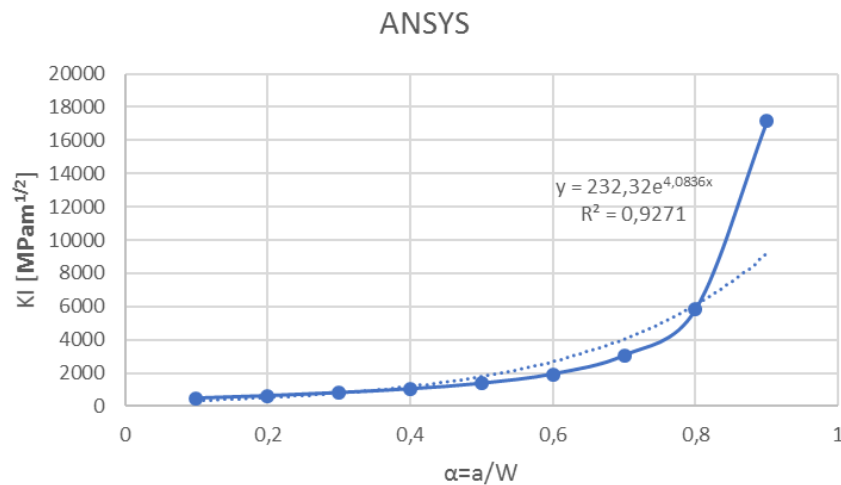
Therefore, for α values of 0.1 to 0.9 in steps of 0.1:



Graph 10-SIF vs. a/W ratio from Knésl and Bednar literature calculations [24].

5.1.3 ANSYS calculations

With the procedure previously explained in item 4 -*Numerical modelling in ANSYS (4.4.1)*- complemented by the item 10.5- *Appendix V-Macro for the CT specimen* and, for α values of 0.1 to 0.9 in steps of 0.1, the K_I results are:



Graph 11-SIF vs. a/W ratio from ANSYS calculations.

5.2 T -stresses

In the following, several graphs are prepared showing the values of the obtained through:

- Knésl and Bednar literature calculations.
- ANSYS calculations.

5.2.1 Knésl and Bednar literature calculations

From Knésl and Bednar [24], the T -stress at the crack-tip, T can be obtained as:

$$T = \frac{K_I B_2}{\sqrt{\pi a}}, \quad (22)$$

where:

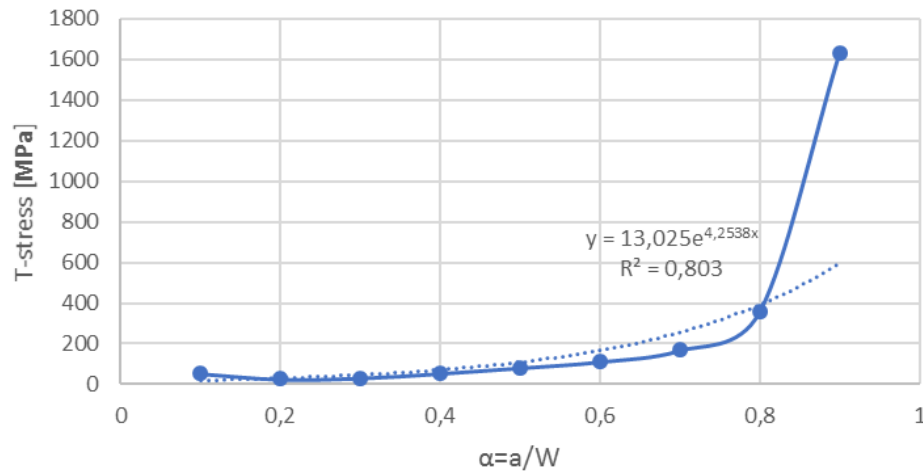
K_I is the stress intensity factor (the values used are the ones obtained in (5.1.2),

B_2 values are given in the literature for each value of the ratio $\alpha = a/W$ and

a is the crack size.

Therefore, for α values of 0.1 to 0.9 in steps of 0.1:

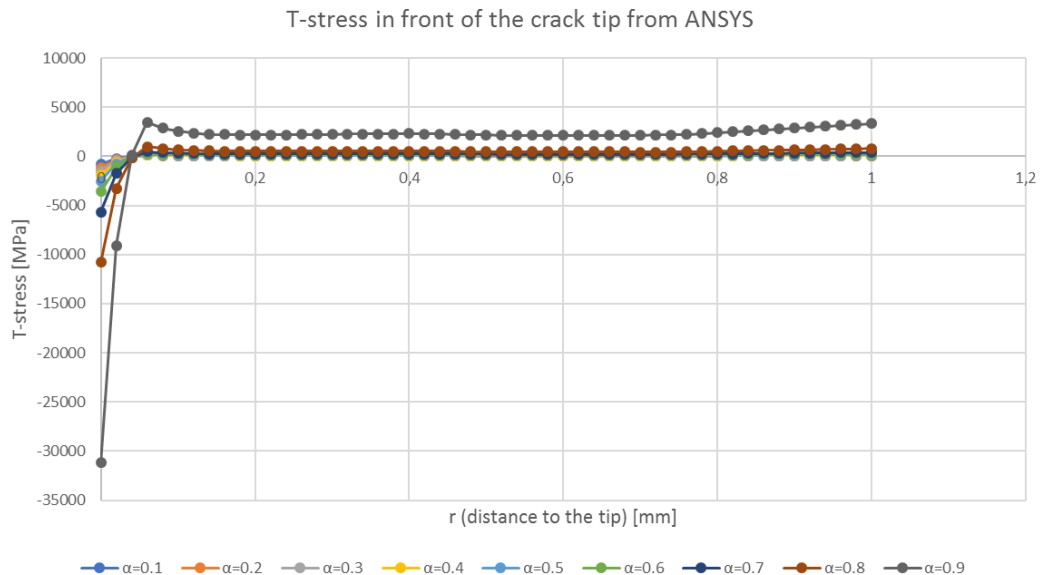
KNĚSL BEDNAR



Graph 12-T-stress vs. a/W ratio from Kněsl and Bednar literature calculations [24]

5.2.2 ANSYS calculations

With the procedure previously explained in item 4 -Numerical modelling in ANSYS (4.4.2)- complemented by the Annex- Macro for the CT specimen, the T -stress results along 1 mm in front of the crack, for α values of 0.1 to 0.9 in steps of 0.1, are (see Graph 13):

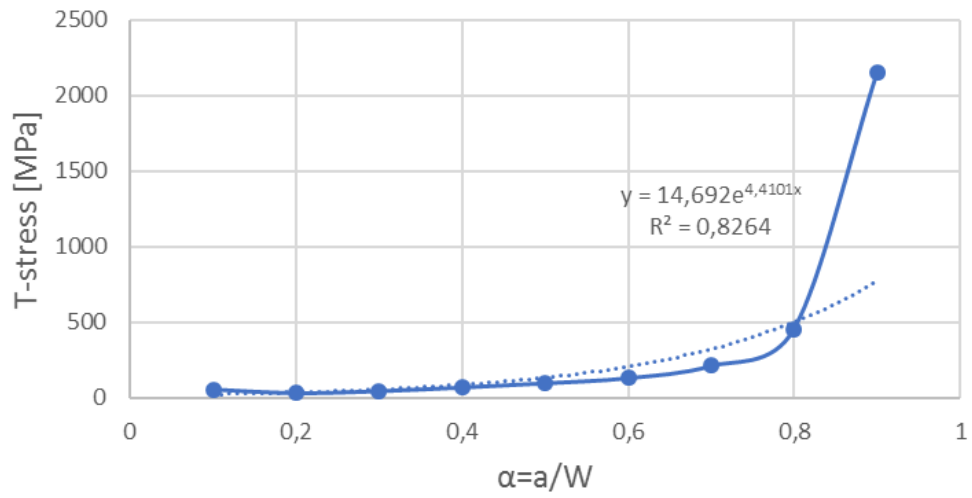


Graph 13-T-stress vs. a/W ratio in front of the crack tip along 1 mm in X-direction from ANSYS calculations.

Because it is necessary to compare with the calculations from Kněsl and Bednar literature and, in that literature, the T -stress is calculated at the crack tip, the values for distance to the tip $r=0$ (i.e. at the crack tip) from Graph 13 must be extracted.

As said in 4.4.2, only the linear part of the graph should be considered, to avoid the deviation observed in the nodes located in the zone near the crack tip. Because of this, instead of extracting the values from $r=0$, the values for $r=0.66$ (in the linear part - see orange zone in Graph 8-) will be considered.

T-stress at r=0.66 mm from ANSYS



Graph 14-T-stress vs. a/W ratio at distance from the tip of $r=0.66$ mm extracted from Graph 13 from ANSYS calculations.

6. VALUES OF S355 PUBLISHED IN LITERATURE

In this item, graphs from S355 steel experiments carried out in several articles are going to be evaluated.

By means of a digitizer software, the graphs that are of interest for this thesis are extracted from those articles and then converted to Excel graphs so that the values can be evaluated.

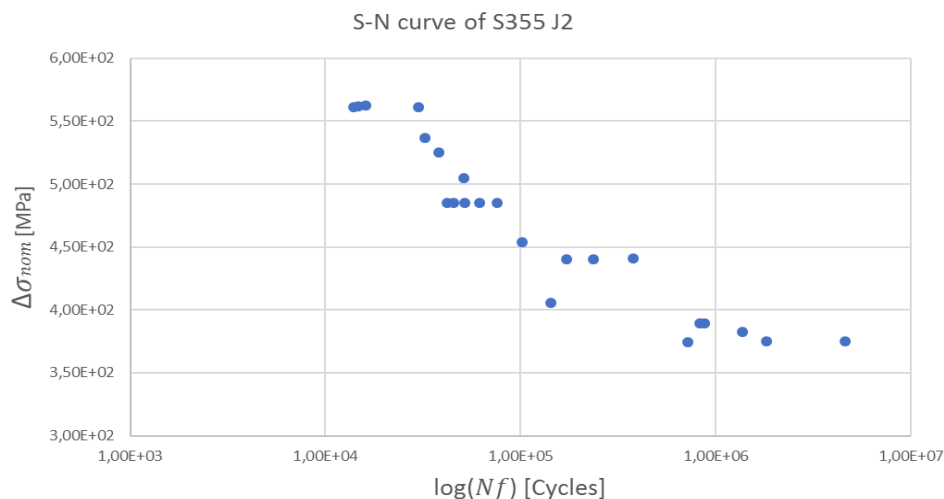
Those experimental graphs are about:

- Stress-Number of Cycles curves.
- Crack propagation rate curves.

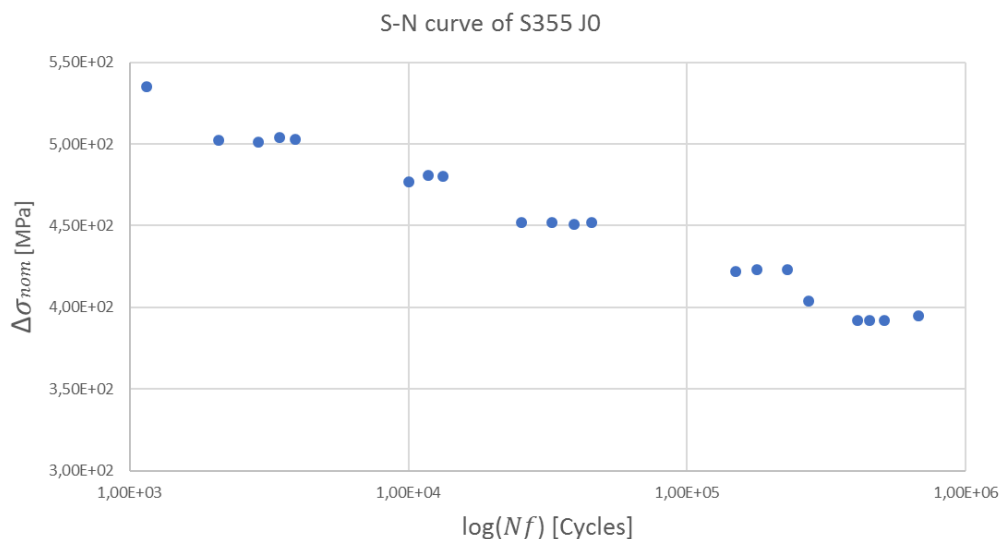
All the graphs are focused in the two different grades considered: S355 J0 and S355 J2.

6.1 Experimental data of $S-N$ curves published in literature

From the point of view of the Wöhler's curves approach, Graphs 15 and 16 are obtained from [25], [26], respectively.



Graph 15-Stress-Number of Cycles curve for S355 J2 from literature. [25]

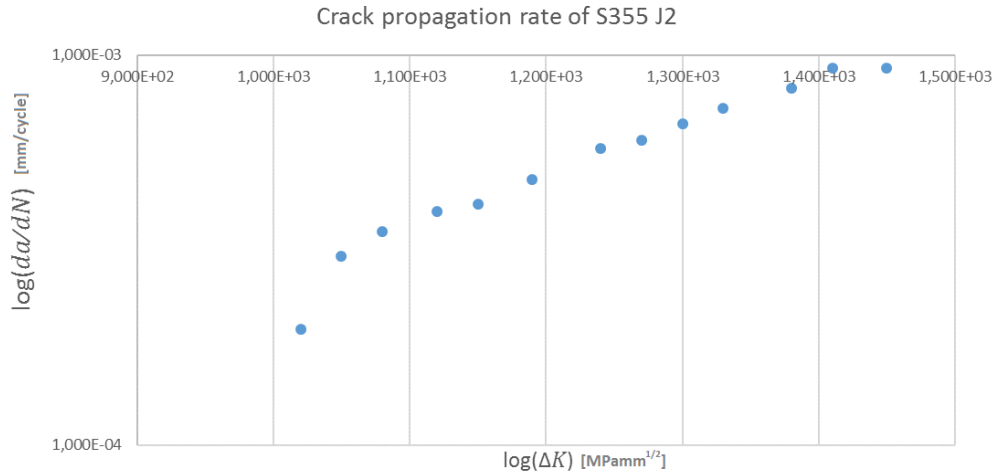


Graph 16-Stress-Number of Cycles curve for S355 J0 from literature. [26]

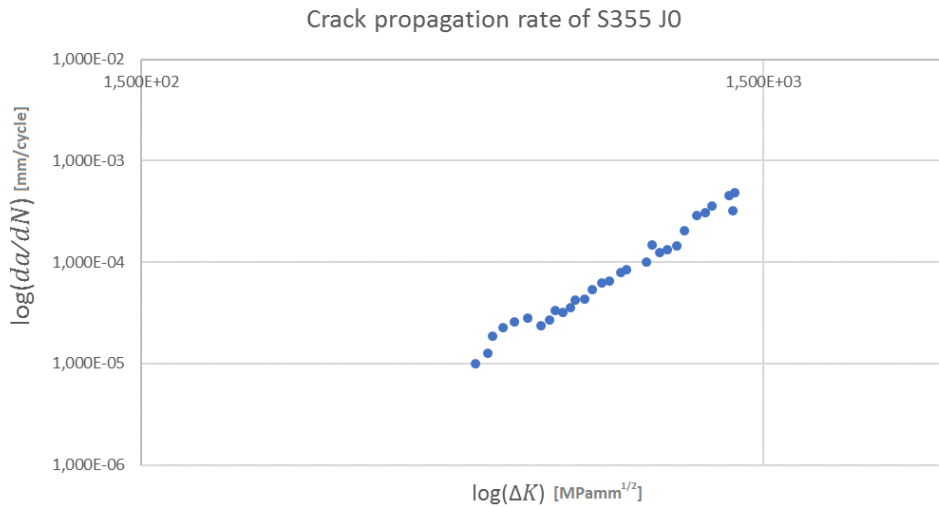
6.2 Experimental data of crack propagation rates published in literature

From the point of view of the fracture-mechanics based approach, Graphs 17 and 18 are obtained from [27], [28], respectively.

As can be shown, only the Paris region is considered.



Graph 17-Crack propagation rate curve for S355 J2 from literature. [27]



Graph 18-Crack propagation rate curve for S355 J0 from literature. [28]

7. EVALUATION OF S355 MEASURED DATA AT INSTITUTE OF PHYSICS OF MATERIALS

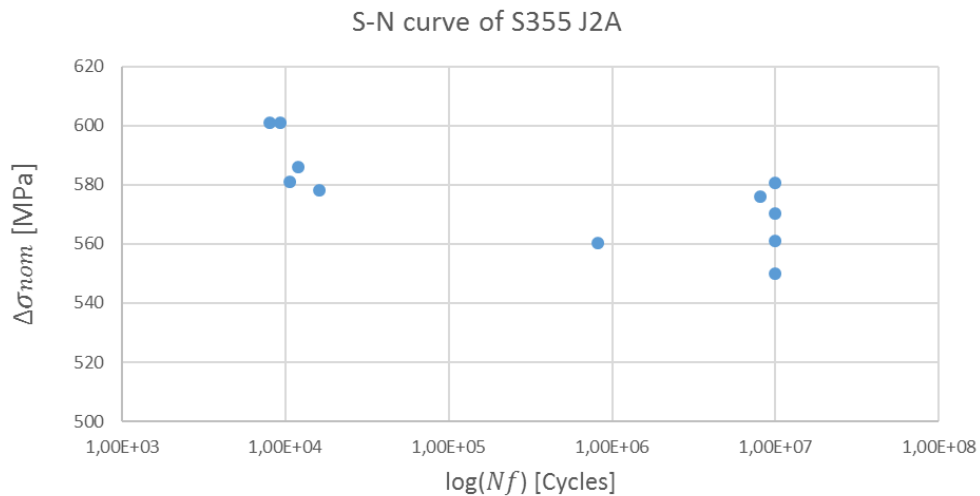
The following graphs are obtained from experiments [29] realized in the Institute of Physics of Materials (IPM) in the Brno University of Technology.

Engineering materials are seldom homogeneous and isotropic. Microstructure, and thus, mechanical properties, are often sensitive to direction of rolling. The sensitivity to orientation is particularly pronounced in fracture toughness measurements, because a microstructure with a preferred orientation may contain planes of weakness, where crack propagation is relatively easy.

The experimental procedure evaluates the fatigue properties depending on the steel grade (J0 and J2) and on the orientation of the CT specimen in the sheet-rolling direction.

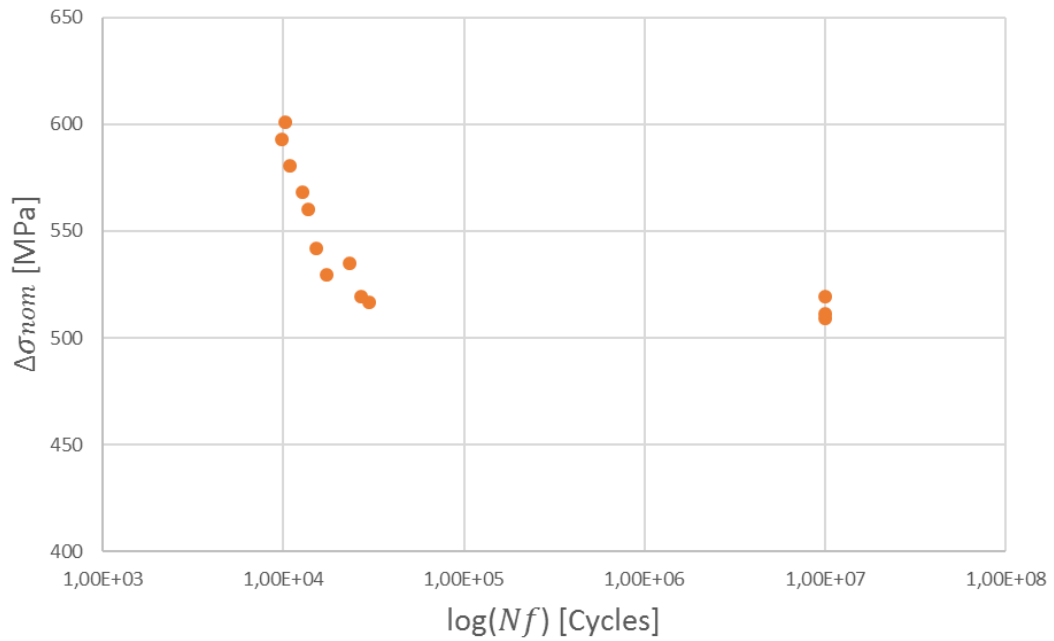
The orientation of the CT specimen in the sheet rolling direction is considered in this way: specimens marked with an "A" (S355_J2A/S355_J0A) means that the crack is propagating in the rolling direction whereas specimens marked with a "B" (S355_J2B/S355_J0B) means that the crack is propagating across to rolling direction.

7.1 Experimental data of $S-N$ curves from IPM



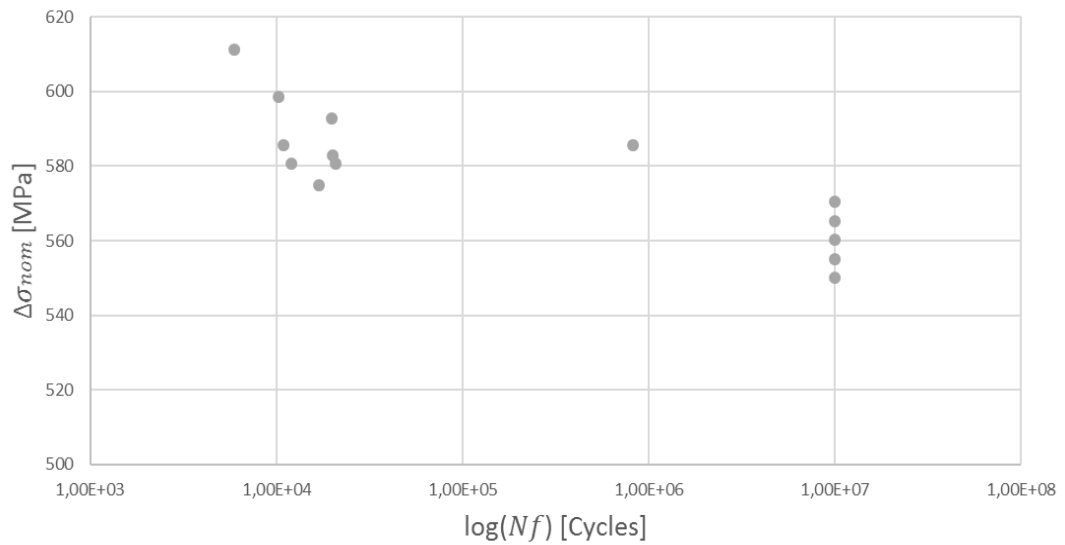
Graph 19-Stress-Number of Cycles curve for S355 J2A from the Institute of Physics of Materials. [29]

S-N curve of S355 J0A



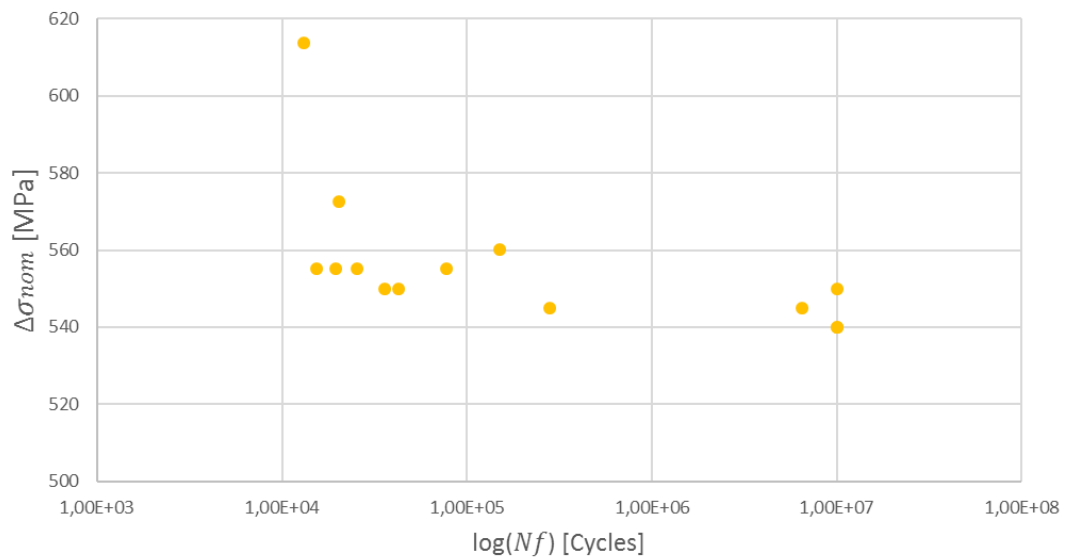
Graph 20-Stress-Number of Cycles curve for S355 J0A from the Institute of Physics of Materials. [29]

S-N curve of S355 J2B



Graph 21-Stress-Number of Cycles curve for S355 J2B from the Institute of Physics of Materials. [29]

S-N curve of S355 J0B

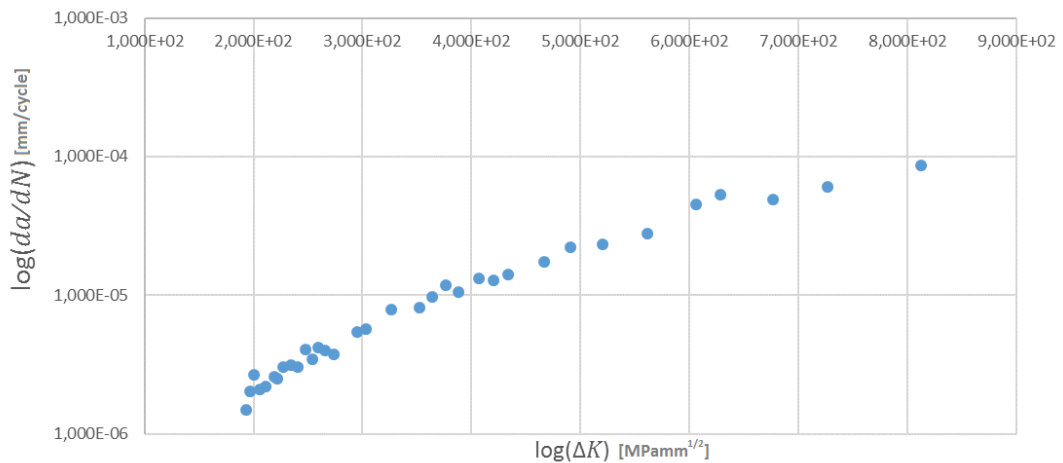


Graph 22-Stress-Number of Cycles curve for S355 J0B from the Institute of Physics of Materials. [29]

7.2 Experimental data of crack propagation rates from IPM

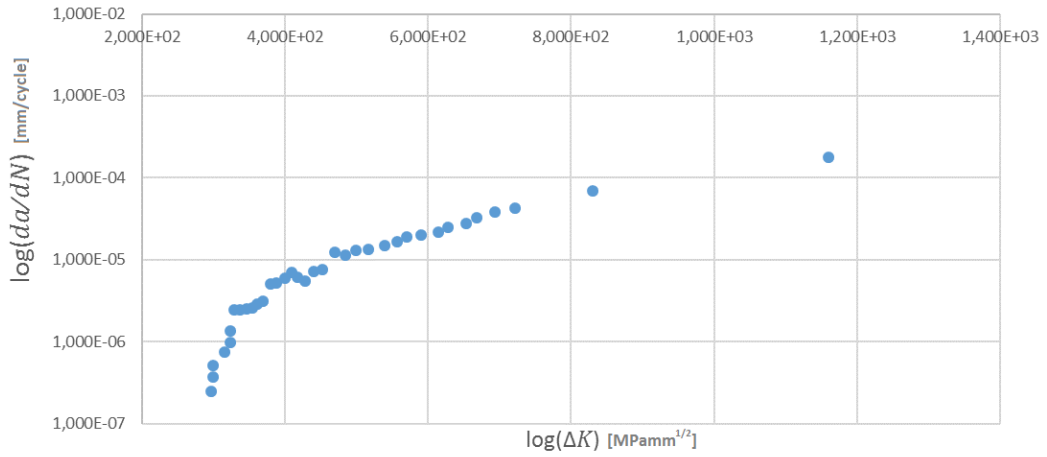
As can be shown, only the Paris region is considered.

Crack propagation rate of S355 J2A



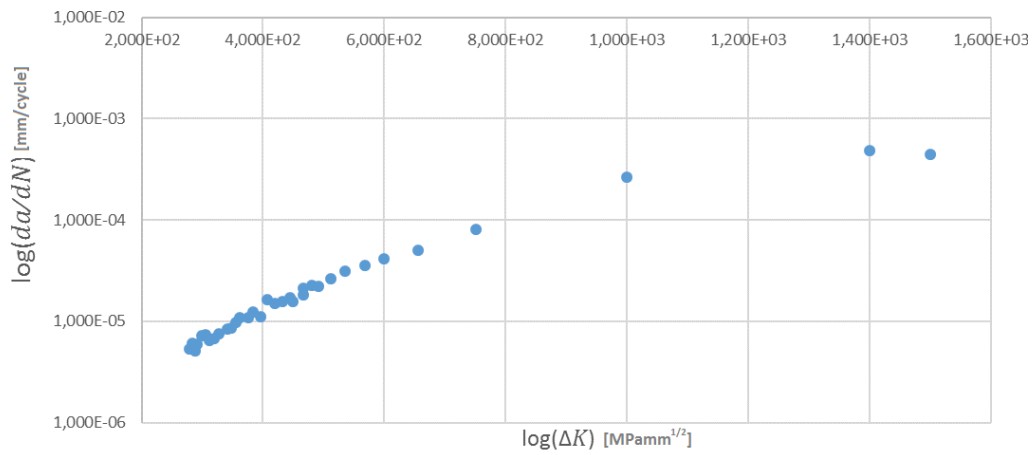
Graph 23-Crack propagation rate curve for S355 J2A from the Institute of Physics of Materials. [29]

Crack propagation rate of S355 J0A

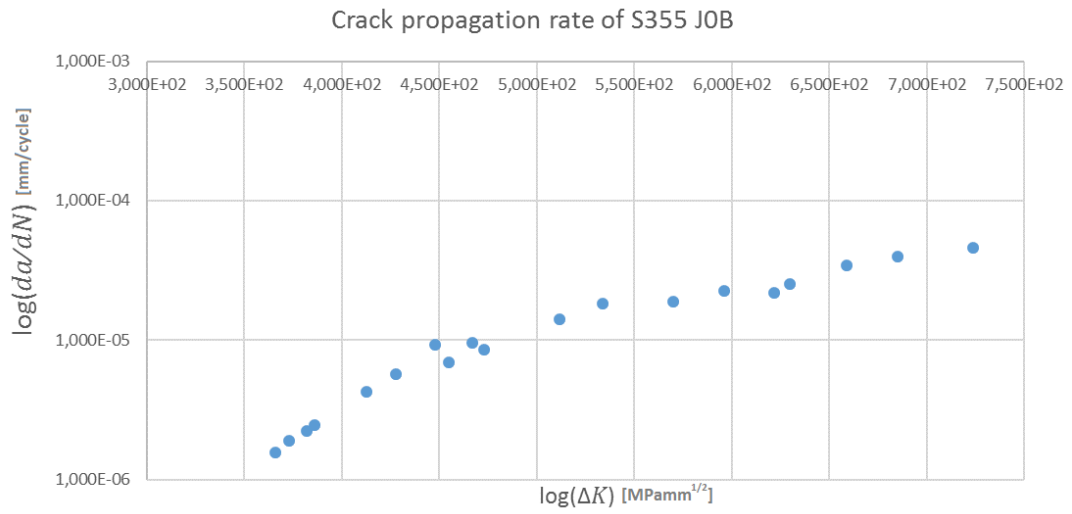


Graph 24-Crack propagation rate curve for S355 J0A from the Institute of Physics of Materials. [29]

Crack propagation rate of S355 J2B



Graph 25-Crack propagation rate curve for S355 J2B from the Institute of Physics of Materials. [29]

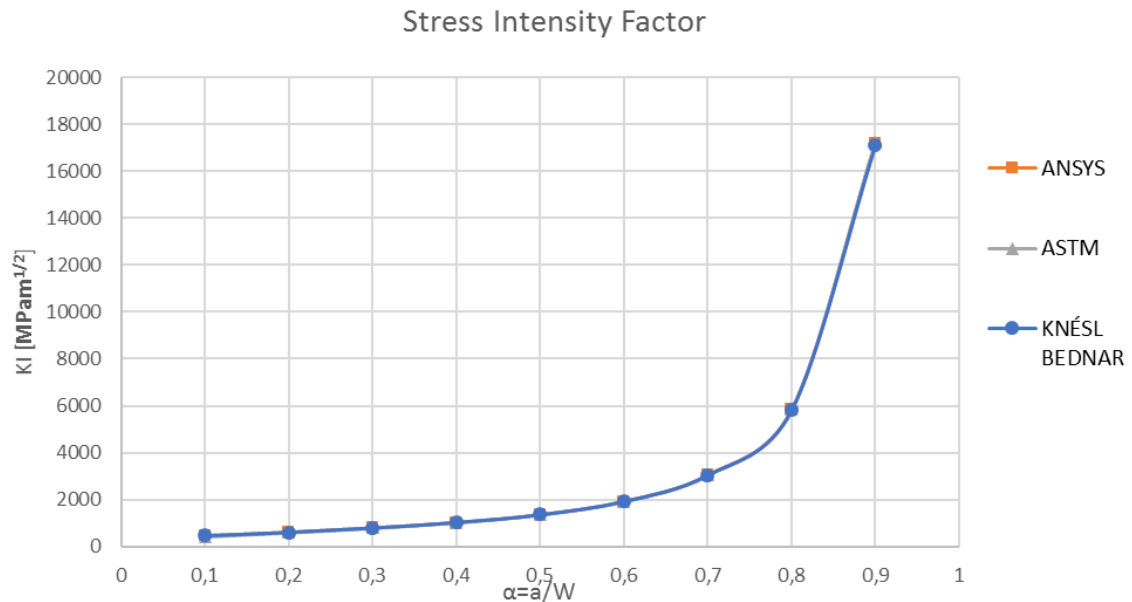


Graph 26-Crack propagation rate curve for S355 J0B from the Institute of Physics of Materials [29].

8. COMPARISON AND DISCUSSION OF THE RESULTS

8.1 Comparison of curves from ANSYS and literature

8.1.1 Comparison of Stress Intensity Factor



Graph 27-Comparison of Stress Intensity Factor from ASTM, KNÉSL AND BEDNAR and ANSYS calculations.

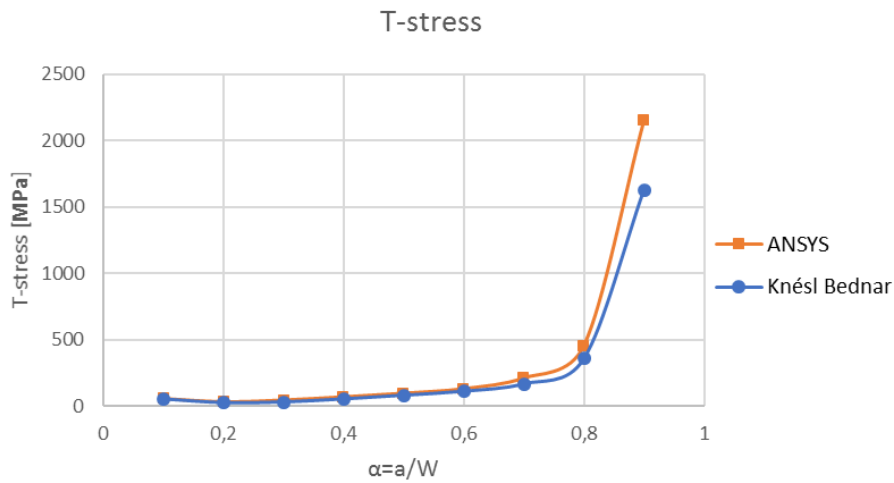
The stress intensity factor increases slowly for low values (until 0.6) of the a/W ratio.

It can be clearly seen, too, that the data for the stress intensity factor are almost coincident for the three polynomial functions considered. The numerical values for a better accuracy can be found in Table 9.

ANSYS	ASTM	KNÉSL
K_I [MPa · m ^{1/2}]	K_I [MPa · m ^{1/2}]	K_I [MPa · m ^{1/2}]
466.14	428.1682592	463.296363
610.36	604.3903178	607.5461464
799.64	794.9144223	795.3537075
1030.5	1029.367866	1026.860468
1364.3	1366	1358.493548
1929.2	1930.987807	1925.027501
3053.4	3047.882974	3046.781699
5829.38	5826.534536	5812.27632
17166	17242.80317	17107.3172

Table 9-Numerical values for the three numerical calculation sources: ANSYS, ASTM and Knésl and Bednar.

8.1.2 Comparison of T -stress

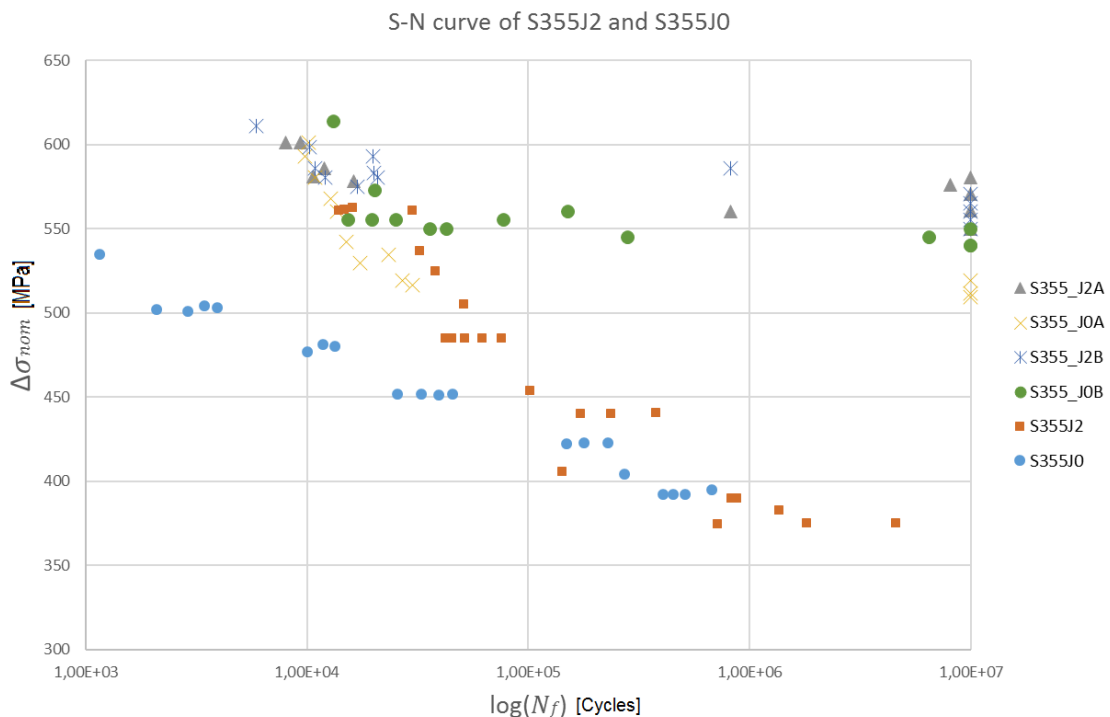


Graph 28-Comparison of T -stress from KNÉSL AND BEDNAR and ANSYS calculations.

The T -stress seems to be very low until higher ratios of a/W are reached (from 0.6).

It is observed an almost coincident regression in T -stress values for α ratios between 0.1 and 0.6. Out from this range, the values differ, obtaining greater values for the ANSYS calculations than the Knésl and Bednar ones.

8.2 Comparison of Stress-Number of cycles curves



Graph 29-Comparison of Stress-Number of Cycles curves from experiment in IPM and experimental data in articles.

Fatigue endurance limit is determined based on the S-N curve where the limit of 10^7 cycles to fracture is usually used to consider the applied stress amplitude as safe for loading during the whole component lifetime.

In this way, it can be observed from Graph 29 that the fatigue endurance limit of the tested grades is:

-S355_J2A: about 570 MPa.

-S355_J2B: about 580 MPa.

-S355J2: about 380 MPa.

-S355_J0A: about 520 MPa.

-S355_J0B: about 550 MPa.

-S355J0: about 400 MPa.

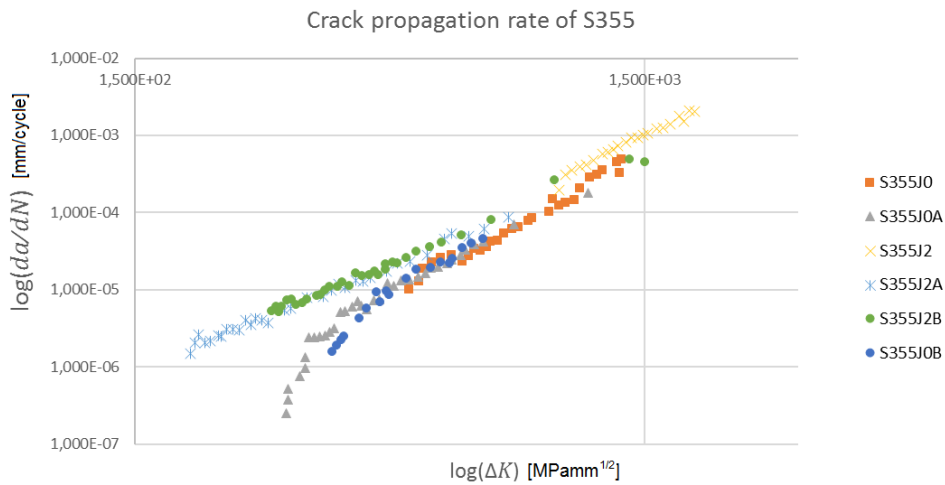
It is necessary to consider that "S355J2" and "S355J0" were probably carried out with different specimens such as round tensile one instead of compact tension (not enough information in the articles about the specimen considered) and maybe due to this, the data plotted for these two grades in that articles is inferior to the values obtained in IPM.

The comparison of fatigue properties (A, B- according the equation (11)) using the Basquin's model from S-N curve is mentioned in Table 10, together with coefficient of determination R^2 .

Steel grade	A	B	R^2
S 355 J0 A	-70.83	1239.1	0.883
S 355 J0 B	-5.01	615.12	0.2183
S 355 J2 A	-7.231	657.12	0.7244
S 355 J2 B	-2.264	610.7	0.0849

Table 10-Fatigue properties of S355 from S-N curve by Basquin's model.

8.3 Comparison of crack propagation rate curves



Graph 30-Comparison of crack propagation rate curves (Paris region) from experiment in IPM and experimental data in articles.

The crack growth rates for all the grades presented differ only slightly, showing a good agreement between the data from articles and the IPM.

In general, crack growth rates are higher for S355 J2 steel grade when compared with S355 J0 grade.

This slight difference could be resulting from the different amount of particles in the material structure and their consequent effect on the crack growth mechanism (explained previously in 2.3.2.1.)

On the other hand, the rolling direction does not have any measurable influence on the crack growth rate, at least in the Paris region, which is the one considered.

The material properties are mentioned for Paris Erdogan law in Table 11.

Steel grade	C	m
S 355 J0 A	2e-15	3.605
S 355 J0 B	2e-15	3.638
S 355 J2 A	2e-12	2.595
S 355 J2 B	1e-12	2.711

Table 11-Fatigue properties of S355 from crack propagation rate versus stress intensity factor – Paris-Erdogan law.

9. CONCLUSIONS

In this thesis, two different parameters for the definition of the crack-tip conditions: *Stress Intensity Factor* and *T-stress*, and two different approaches to fatigue analysis (in two different S355 grades): statistics (*Wöhler's curve*) and Fracture Mechanics (*Crack Propagation Rate curve*), were evaluated and compared with experimental data and data from literature.

The following conclusions can be drawn:

- The three formulas (polynomial functions) for the calculation of the SIF (ANSYS, ASTM, Knésl and Bednar) show a very good agreement between them.
- ANSYS' and Knésl and Bednar's obtained values seem to be a good approach for the calculation of the *T-stress* at the crack tip since they show a good agreement between them.
- In general, S355 J2 grade exhibit a greater fatigue-endurance limit.
- There is none appreciable difference between the fatigue-endurance limits of specimens with the same grade but different rolling direction.
- The S355 J2 steel grade exhibits higher crack growth rates when compared with the S355 J0 steel grade.
- The crack growth rate seems to be independent of the rolling direction and, thus, resulting structure.
- Both *S-N* and $da/dN-\Delta K$ curves seem to be influenced only by the different chemical composition of the considered steel grades.

10. APPENDIX

10.1 APPENDIX I - Nomenclature

a	Crack size
FE	Finite Elements
K or SIF	Stress Intensity Factor
K_I	Stress Intensity Factor (Mode I)
P	Load applied
r	Distance from the crack tip (Cartesian coordinate)
B or t	Thickness of the specimen
θ	Angular coordinate
σ_{YS}	Yield Strength
σ or S	Stress
$LEFM$	Linear Elastic Fracture Mechanics
$EPFM$	Elastic Plastic Fracture Mechanics
$CTOD$ or δ	Crack Tip Opening Displacement
CT	Compact Tension
ν	Poisson's ratio
E	Young's modulus
W	Width of specimen
T	T -stress
ρ	Density
UTS	Ultimate Tensile Strength
K_{Ic}	Critical value of the Stress Intensity Factor (Fracture toughness)
ΔK	Stress Intensity Factor range
LCF	Low Cycle Fatigue
HCF	High Cycle Fatigue
N	Number of cycles

10.2 APPENDIX II - List of figures

Figure 1-Definition of the coordinate system with origin in crack tip: Polar and Cartesian. [9].....	8
Figure 2-The three modes of loading that a crack can experience. [9].....	9
Figure 3-Definition of Polar coordinates with $\theta = 0$ [9].....	10
Figure 4-Alternative definitions of CTOD: (a) displacement at the original crack tip and (b) displacement at the intersection of a 90° vertex with the crack flanks. [9]	11
Figure 5-Small-scale yielding condition. [9]	13
Figure 6-Typical fatigue fracture appearance.....	15
Figure 7-Stages of the lifecycle of a fatigue crack. [11]	15
Figure 8-Crack nucleation from inclusions. [2].....	16
Figure 9-Microstructurally short crack. [11].....	17
Figure 10-Mechanically short crack. [11]	18
Figure 11-Long crack. [11].....	18
Figure 12-Typical CT specimen [21].....	24
Figure 13-CT dimensions. [22].....	25
Figure 14-Apparatus for testing CT specimens. [9]	26
Figure 15-List of some of the element types available in ANSYS.	31
Figure 16-PLANE82, 2-D, 8-Node, Structural Solid. [23].....	32
Figure 17-Linear isotropic properties for steel. Young's modulus (EX) [MPa] and Poisson's number (NUXY) [-].....	33
Figure 18-Plane of symmetry (in red) considered.....	33
Figure 19-KP of the specimen numerated.	34
Figure 20-Detailing of the KP at the crack tip.....	34
Figure 21-Lines of the specimen numerated.	35
Figure 22-Detailing of the lines at the crack tip.....	35
Figure 23-Areas of the specimen numerated.	36
Figure 24-Detailing of the areas at the crack tip.	36
Figure 25-Meshing of the specimen.	37
Figure 26-Detailing of the concentrated meshing around the tip.....	37
Figure 27-All boundary conditions applied upon the specimen.....	38
Figure 28-Stress intensity [MPa] around the tip for $a/W=0.5$ and deformed crack tip... 39	39
Figure 29-Deformed shape for $a/W=0.5$	39
Figure 30-KI calculation in ANSYS for $a/W=0.5$	40
Figure 31-Path established (in red) for the calculation of KI and schematic representation including Polar and cartesian coordinates for the considered model (half-crack).....	40
Figure 32-Selection of the nodes in 1 mm in front of the crack tip.....	41
Figure 33-Example of list from ANSYS solution with the distance to the tip (S), σ_{xx} (SX) and σ_{yy} (SY).	41

10.3 APPENDIX III - List of tables

Table 1-Basic grade designation for category 1 steels.	27
Table 2-Impact and temperature codes for structural steels, category 1.....	27
Table 3-Delivery condition codes for structural steels, category 1.....	28
Table 4-Chemical composition of S355.	28
Table 5-Yield Strength for S355.....	29
Table 6-Ultimate strength for S355.	29
Table 7-Chemical composition in percentage by weight of steel grade S355 J2 according to EN 10025-2:2004 standard.....	29
Table 8-Chemical composition in percentage by weight of steel grade S355 J0 according to EN 10025-2:2004 standard.....	29
Table 9-Numerical values for the three numerical calculation sources: ANSYS, ASTM and Knésl and Bednar.....	55
Table 10-Fatigue properties of S355 from S-N curve by Basquin's model.	57
Table 11-Fatigue properties of S355 from crack propagation rate versus stress intensity factor – Paris- Erdogan law.....	58

10.4 APPENDIX IV - List of graphs

Graph 1-Fatigue regimes.....	12
Graph 2-Constant amplitude fatigue crack growth. [9]	13
Graph 3-Crack propagation stages including the thresholds of fatigue. [11].....	17
Graph 4-Typical (long) fatigue crack growth behavior in metals. [9].....	19
Graph 5-Typical S–N curves including the VHCF-region: (a) low strength steels, components with sharp notches (b) materials with body-centered cubic lattice under corrosive media or at elevated temperatures, materials with face-centered cubic lattice (c) some high strength steels, components with surface treatment (d) high and very high strength steels, materials with face-centered cubic lattice. [13].....	21
Graph 6-S-N field with percentile curves representing the same probability of failure. [14]	23
Graph 7-Schematic representation of the Kohout-Věchet S-N curve. [20].....	24
Graph 8-Example of regression for the T -stress in front of the crack for $a/W=0.5$	42
Graph 9-SIF vs. a/W ratio from ASTM literature calculations [22].	43
Graph 10-SIF vs. a/W ratio from Knésl and Bednar literature calculations [24].....	44
Graph 11-SIF vs. a/W ratio from ANSYS calculations.....	45
Graph 12- T -stress vs. a/W ratio from Knésl and Bednar literature calculations [24].....	46
Graph 13- T -stress vs. a/W ratio in front of the crack tip along 1 mm in X-direction from ANSYS calculations.....	46
Graph 14- T -stress vs. a/W ratio at distance from the tip of $r=0.66$ mm extracted from Graph 13 from ANSYS calculations.....	47
Graph 15-Stress-Number of Cycles curve for S355 J2 from literature. [25]	48
Graph 16-Stress-Number of Cycles curve for S355 J0 from literature. [26]	48
Graph 17-Crack propagation rate curve for S355 J2 from literature. [27]	49
Graph 18-Crack propagation rate curve for S355 J0 from literature. [28]	49
Graph 19-Stress-Number of Cycles curve for S355 J2A from the Institute of Physics of Materials. [29].....	50
Graph 20-Stress-Number of Cycles curve for S355 J0A from the Institute of Physics of Materials. [29].....	51
Graph 21-Stress-Number of Cycles curve for S355 J2B from the Institute of Physics of Materials. [29].....	51
Graph 22-Stress-Number of Cycles curve for S355 J0B from the Institute of Physics of Materials. [29].....	52
Graph 23-Crack propagation rate curve for S355 J2A from the Institute of Physics of Materials. [29].....	52
Graph 24-Crack propagation rate curve for S355 J0A from the Institute of Physics of Materials. [29].....	53
Graph 25-Crack propagation rate curve for S355 J2B from the Institute of Physics of Materials. [29].....	53
Graph 26-Crack propagation rate curve for S355 J0B from the Institute of Physics of Materials [29].....	54

Graph 27-Comparison of Stress Intensity Factor from ASTM, KNÉSL AND BEDNAR and ANSYS calculations.....	55
Graph 28-Comparison of T -stress from KNÉSL AND BEDNAR and ANSYS calculations.	56
Graph 29-Comparison of Stress-Number of Cycles curves from experiment in IPM and experimental data in articles.	56
Graph 30-Comparison of crack propagation rate curves (Paris region) from experiment in IPM and experimental data in articles.	58

10.5 APPENDIX V - Macro for the CT specimen

10.5.1 Prior setup

```
/title,compact tension specimen
/replot
finish
/output,,tmp
WPCSYS,-1,0
/clear
/output
/COLOR,ELEM,BLUE
/COLOR,OUTL,WHIT
/replot
/PNUM,KP,1
/PNUM,LINE,1
/PNUM,AREA,1
/filnam,CTspecimen
```

10.5.2 Preprocessor

```
/prep7
!*****
! PARAMETERS
!*****
pi=3.1415926535897932384626433832795
W=50
a_W=0.5
a=a_W*W

!*****
! ELEMENT DEFINITION
!*****

ET,1,PLANE82
KEYOPT,1,3,2

!*****
! MATERIAL DEFINITION
!*****

MP,EX,1,210000
MP,NUXY,1,0.3

!*****
! BUILT OF THE SPECIMEN
!*****

! -----KEYPOINTS-----
k,1,0,0
K,2,0,1
k,3,1,0
```

k,4,-1,0
 k,5,a+0.25*W,0
 k,6,a+0.25*W,0.6*W
 k,7,-(W-a),0.6*W
 k,8,-(W-a),0
 k,9,a,0.4*W
 k,10,a-0.125*W,0.275*W
 k,11,a,0.15*W
 k,12,a+0.125*W,0.275*W
 k,13,a,0.275*W

! -----LINES-----

L,1,3 ! L1
 L,1,2 ! L2
 L,1,4 ! L3
 Larc,3,2,1,1 ! L4
 Larc,2,4,1,1 ! L5
 L,3,5 ! L6
 L,5,6 ! L7
 L,6,7 ! L8
 L,7,8 ! L9
 L,8,4 ! L10
 Larc,9,10,13,0.125*W ! L11
 Larc,10,11,13,0.125*W ! L12
 Larc,11,12,13,0.125*W ! L13
 Larc,12,9,13,0.125*W ! L14
 L,5,11 !L15
 L,7,10 !L16

! -----AREAS-----

a1,1,2,4 !A1
 a1,2,3,5 !A2
 a1,6,15,12,16,9,10,5,4 !A3
 a1,15,13,14,11,16,8,7 !A4

!*****

! MESHING

!*****

Kscon,1,0.05,1,4,0.75

kESIZE,1,1
 kESIZE,2,1
 kESIZE,3,1
 kESIZE,4,1
 kESIZE,5,1
 kESIZE,6,5
 kESIZE,7,5
 kESIZE,8,1
 kESIZE,9,5
 kESIZE,10,5

kESIZE,11,5
 kESIZE,12,5
 kESIZE,13,5

!Material
 TYPE,1
 MAT,1

AMESH,1
 AMESH,2
 AMESH,3
 AMESH,4

FINISH

10.5.3 Solve

!*****
 ! BOUNDARY CONDITIONS
 !*****

!-----SYMMETRY-----

/solu
 NSEL,S,LOC,X,0,-(W-a)
 NSEL,R,LOC,Y,0,0
 DSYM,SYMM,y, ,

allsel, all

!-----SUPPORTS-----

NSEL,S,LOC,X,a,a
 NSEL,R,Loc,y,0.4*W,0.4*W
 D,all, ,0, , , ,Ux, , , , ,

allsel,all
 eplot

!-----LOADS-----

FK,9,FY,1000

allsel,all
 eplot
 solve

FINISH

10.5.4 Postprocessing

10.5.4.1 Calculation of SIF

/POST1

eplot

LPATH,1,3,4

KCALC,0,1,0,0

10.5.4.2 Calculation of T-stress (along 1 mm in front of the crack)

*NOTE: the procedure was made by means of the GUI.

NSEL,S,LOC,X,-1,0

NSEL,R,LOC,Y,0,0

nplot

/POST1

FLST,2,2,1

FITEM,2,1

FITEM,2,118

PATH,Tstress1,2,50,50,

PPATH,P51X,1

PATH,STAT

/REPLOT,RESIZE

AVPRIN,0, ,

PDEF, ,S,X,AVG

/PBC,PATH, ,0

AVPRIN,0, ,

PDEF, ,S,Y,AVG

/PBC,PATH, ,0

PRPATH,SX,SY

11. REFERENCES

- [1] P.-a. H. Wirsching, Statistical summaries of fatigue data for design purposes, NASA contractor report.
- [2] J. Belzunce, Tecnología de materiales-Comportamiento en servicio de materiales, University of Oviedo, 2012.
- [3] W. A. J. Albert, Uber Treibseile am Harz, Archiv fur Mineralogie Geognosie Bergbau und Huttenkunde, 1838.
- [4] A. A. Griffith, The phenomena of rupture and flow in solids, 1921.
- [5] E. Paris P. C., A critical analysis of crack propagation laws, J. Basic Eng., 1963.
- [6] W. Weibull, A Statistical Theory Of The Strength Of Materials, Stockholm, 1939.
- [7] ASTM, Symposium on Fatigue With Emphasis on Statistical Approach, June 1952.
- [8] ASTM, Symposium on Statistical Aspects of Fatigue, June 1951.
- [9] P. T.L Anderson, Fracture Mechanics: fundamentals and applications, Boca Raton: Taylor & Francis group, Third edition-2005.
- [10] A. F. Canteli, A statistical model for crack growth based on tension and compression Wöhler fields, -: Elsevier Ltd., 2008.
- [11] e. a. Zerbst U, Fatigue strength and fracture mechanics – A general perspective., Berlin: Elsevier Ltd.- Engng Fract Mech., 2017.
- [12] ASTM, ASTM Standard Test Method For Measurement of Fatigue Crack Growth Rates, West Conshohocken, PA, 1999.
- [13] A. F. Canteli, Comparison of different statistical models for description of fatigue including very high cycle fatigue, 2016.
- [14] E. Castillo, Using statistical compatibility to derive advanced probabilistic fatigue models, 2010.
- [15] E. F. C. A. Castillo, A general regression model for lifetime evaluation and prediction., Int. Journal of fracture, 2001.
- [16] E. L.-A. M. R. A. F.-C. A. E. V. K. R. Castillo, Length effect on the fatigue strength of prestressing wires and strands. Analysis of the independence model., Int. J. of Fatigue.
- [17] E. F.-C. A. H. A. Castillo, On fitting a fatigue model to data., Int. J. of Fatigue, 1999.
- [18] O. M. D. R. T. K. Chaminda SS, Different approaches for remaining fatigue life estimation of critical members in railway bridges., 2007.
- [19] J. K. R., A new approach for estimating fatigue life in offshore steel structures, Stavanger, Norway: Faculty of Science and Technology: MSc. Thesis..
- [20] A. C. J.A.F.O. Correia, A generalization of the fatigue Kohout-Vechet model for several fatigue damage parameters, Elsevier, 2017.
- [21] en.wikipedia.org.

- [22] ASTM, Standard test method for measurement of fracture toughness.
- [23] ANSYS, "Mechanical APDL Element Reference".
- [24] B. S. S. Knésl, Values of the first four coefficients of the William's expansion for basic types of mechanical fracture testing bodies (in Czech language), Brno: Institute of Physics of Materials, Academy of sciences.
- [25] P. S. Tomas Tomaszewski, Analytical models of the S-N curves based on the hardness of the material, Funchal, Madeira, Portugal: 2nd International Conference on Structural Integrity, ICSI 2017. Elsevier, 4-7 September 2017.
- [26] G. SZALA, Stress sensitivity coefficient of a material in the range of high-cycle fatigue, University of Technology and Life Sciences, Bydgoszcz, Poland.
- [27] O. Adepipe, Review of corrosion fatigue in offshore structures: Present status and challenges in offshore wind sector, Renewable and Sustainable Energy Reviews., 2016.
- [28] A. M. P. De Jesus, A comparison of the fatigue behavior between S355 and S690 steel grades, Journal of construction Steel Research, 2012.
- [29] S. SEITL, Comparison of the Fatigue Crack Propagation Rates in S355 J0 and S355 J2 Steel Grades, Brno, Czech Republic: Key Engineering Materials in Press.
- [30] ANSYS, Mechanical APDL command reference.
- [31] ANSYS, Mechanical APDL theory reference.
- [32] A. J. Contreras, "Comportamiento a fatiga de los materiales," Engineering & Materials, 2014. [Online]. Available: <https://materialsbreakthroughs.wordpress.com>.
- [33] E. Castillo, A new probabilistic model for crack propagation under fatigue loads and its connection with Wöhler fields., -: Elsevier Ltd., 2009.
- [34] E. Castillo, Comparative analysis of two models for evaluating fatigue data., 2009.
- [35] E. 10025-2:2004, European standard for hot-rolled structural steel. Part 2- Technical delivery conditions for non-alloy structural steels.
- [36] E. 1. E. Standard, S355 Standard Structural Steel Plate, 2004.

12. CURRICULUM VITAE

PERSONAL INFORMATION

- Name: Álvaro Martín González
- Birth: May 16, 1996 (22 years)
- Place of birth: Oviedo (Asturias), Spain
- ID: 71738151-R
- Address: Manuel Fernández Avello St, no. 6, 5-A, 33011, Oviedo, Spain.
- Phone numbers: +34 616759981, +34 985114615
- E-mail: alvaro_martin_gonzalez@hotmail.com



STUDIES

- Mechanical Engineering bachelor taught in English (4 years) with a mention in construction at *University of Oviedo - Gijón Polytechnic School of Engineering* (2014-2018)
- *Erasmus+* mobility (1 year) in *Brno University of Technology* (Faculty of Civil Engineering), Brno, Czech Republic (2017-2018). Taking the courses of the last academic year including the Final Bachelor Thesis.
- Technological baccalaureate (2 years) at *Colegio Loyola P.P. Escolapios*, Oviedo (Asturias), Spain (2012-2014).
- Secondary Education (4 years) at *Colegio Loyola P.P. Escolapios*, Oviedo (Asturias), Spain (2008-2012).

LANGUAGES

- Spanish: native.
- English: Trinity College London – B2.

COMPUTER SKILLS

- Medium-to-high level: AutoCad, ANSYS, LISAFEA, Autodesk Inventor, CESPLA.
- Medium-to-high level: Microsoft Office (Word, Excel, PowerPoint, Access).
- Basic Formation: EES, Matlab, Wxmaxima.

APTITUDES AND PERSONAL SKILLS

- Work-in-team capability.
- Leadership capability.
- Effort, perseverance and dedication.
- Adaptive capability.
- Good presence.

ADDITIONAL INFORMATION

- European Driving License – B (Spain).
- Own car, willingness to travel.